# NUMERICAL SIMULATION OF COMMINUTION IN GRANULAR MATERIALS WITH AN APPLICATION TO FAULT GOUGE EVOLUTION

A Thesis

by

RICHARD ANTHONY LANG

Submitted to the Office of Graduate Studies of
Texas A&M University
in partial fulfillment of the requirements for the degree of

MASTER OF SCIENCE

May 2002

Major Subject: Geophysics

# NUMERICAL SIMULATION OF COMMINUTION IN GRANULAR MATERIALS WITH AN APPLICATION TO FAULT GOUGE EVOLUTION

A Thesis

by

RICHARD ANTHONY LANG

Submitted to Texas A&M University
in partial fulfillment of the requirements
for the degree of

MASTER OF SCIENCE

Approved as to style and content by:

| | |
|---|---|
| David Sparks<br>(Chair of Committee) | Brann Johnson<br>(Member) |
| Andrew Hajash<br>(Member) | Peter Valkó<br>(Member) |
| Andrew Hajash<br>(Head of Department) | |

May 2002

Major Subject: Geophysics

# ABSTRACT

Numerical Simulation of Comminution in Granular

Materials with an Application to

Fault Gouge Evolution. (May 2002)

Richard Anthony Lang, B.S., University La Sapienza

Chair of Advisory Committee: Dr. David Sparks

The majority of faults display a layer of crushed wear material ("fault gouge") between the fault blocks, which influences the strength and stability of faults. This thesis describes the results of a numerical model used to investigate the process of comminution in a sheared granular material. The model, based on the Discrete Element Method, simulates a layer of 2-D circular grains subjected to normal stress and sheared at constant velocity. An existing code was modified to allow grains to break when subjected to stress conditions that generate sufficient internal tensile stresses. A suite of five numerical runs was performed using the same initial system of grains with sizes randomly chosen from a pre-defined Gaussian distribution. A range of confining pressures was explored from 4.5 MPa to 27.0 MPa (in case of quartz grains with average diameter of 1 mm). The average effective friction coefficients of the five simulations were relatively unaffected by comminution and displayed a constant value of about 0.26. The amount of breakage was directly related to both the applied confining pressure and logarithm of the displacement along the fault. The particle size distribution evolved

during the runs, but it was apparently determined only by the cumulative number of grain breakage events: two runs with the same number of breakage events had identical particle size distributions, even if they deformed to different extents under different stress conditions. These results suggest that the knowledge of both the local displacement and stress state on a fault can be used to infer the local particle size distribution of the gouge.

# DEDICATION

To my wonderful wife Rosa

Who has supported me through

this endeavor with constant love.

# ACKNOWLEDGEMENTS

My gratitude goes, first of all, to my advisor David Sparks, and to all my committee members: Brann Johnson, Andy Hajash, and Peter Valkó from the Petroleum Engineering Department. Special thanks go to Anthony Gangi for the numerous discussions with him, which have been great stimuli for the research. Finally, I want to thank Chris Ieronimus for finding and bringing to my attention Muskhelishvili's solution.

# TABLE OF CONTENTS

Page

Page

# LIST OF FIGURES

FIGURE Page

# LIST OF TABLES

# INTRODUCTION

The mechanical behavior of heterogeneous granular media under normal and shear stresses has been for years one of the principal topics of research in Earth Sciences, as well as in Physics and Material Sciences, because of the wide variety of both natural and man-made granular materials. For example, the majority of seismogenic faults display a layer of crushed wear material ("fault gouge") between the fault blocks, which influences the frictional behavior of the faults. This influence is the reason why much emphasis is given to the process of cataclasis, the evolution of the particle size distribution (PSD), and the microstructures within the layer of fault gouge. Laboratory experiments try to emulate shearing of granular materials providing insight into these processes, but it is difficult to fully capture the detailed evolution of the granular media. As an example of our limited knowledge, let's consider Kanamori's "Asperity Model" of faults [see Scholz, 1990 for summary]. In this model, the high moment releases associated with earthquakes are the result of "strong" areas ("asperities") along faults at which failure initiates and from which it propagates to the entire fault surface. Assuming that the model is correct for bare surface faults, can we find analogues to asperities along gouge-filled faults where the granulated rock is much weaker than the intact country rock? How can we describe this type of asperity?

---

This thesis follows the style and format of *Journal of Geophysical Research*.

The importance of understanding the role of gouge evolution is not limited to the frictional behavior of faults. For instance, Pittman [1981] discussed small gouge-filled-faults in quartz sandstone of the Simpson Group (Oklahoma, USA) revealing that, in addition to stratigraphic and compositional contrasts (shale against sandstone), contrasts in texture (and in particular grain size) can also act as seals for hydrocarbons. In this regard, Berg and Avery [1995] pointed out that slightly cemented (1-14% cement) fine-grained gouges might exhibit high displacement pressures (the pressure of the column of hydrocarbons needed to displace the water from the pore space) and, therefore behave as effective seals. Ultimately, the detailed knowledge or prediction of the PSD evolution in a gouge is a prerequisite for evaluating sealing properties of faulted clastic reservoir rocks.

These are just two examples of the interesting problems related to fault gouge evolution. However, this thesis will address neither of the two specific examples, but it will instead try to answer more basic questions. In the last decade or so, the exponential growth of machine computing power and the development of accurate algorithms have fostered various numerical studies which had the objective of gaining more insights in the mechanical behavior of granular media. It is on the basis of such studies that new subroutines were designed and implemented in the code Granfrixl, to effectively simulate grain breakage in a layer of 2-D circular grains under shear and normal stresses. In particular, the thesis focuses on the evolution of grain breakage with displacement in a fault gouge and how such evolution affects the texture and frictional properties of the gouge itself.

# PREVIOUS WORK

Several researchers from various disciplines have used different approaches to study the rather complex behavior of granular materials subjected to external forces. There is much research on the mechanics of grain comminution and the evolution of the particle size distribution within deforming granular materials. In this review, emphasis will be given to research in the geological and Physics literature, but also to results from the engineering literature related to powder technology.

Engelder [1974] described naturally and experimentally deformed samples of fault gouges, in which some large original grains tend to survive cataclasis (i.e. "granulation of grains by fracturing and rigid-body rotation") and become incorporated by a fine-grained cataclastic matrix. Mandl et al. [1977] also observed that, at the end of their experiments on a variety of granular materials (including glass spheres, pyrex glass grains and splinters, sugar, ground walnut shells, and rounded sand) in a ring-shear apparatus, a high fraction of the large grains embedded in fine material survived cataclasis. Other authors, who reported similar textures, attributed them to several possible causes. Prasher [1987] mentioned a series of experiments performed by Hoffmann & Schönert [1971], which demonstrated that the breakage probability of larger grains in a binary mixture of spheres is reduced when the number of contact points per grain (coordination number) is increased. Sammis et al. [1987], in their "constrained comminution" model, proposed that a grain's fracture probability depends on the relative size of its near neighbors such that grains in contact with grains of similar size are the

"next to break". Cladouhos [1999], analyzing samples of naturally deformed fault gouge and breccia from Death Valley, California, invoked a "cushioning" effect of surrounding small grains on large survivor grains and suggested that grain fracture was minimal during advanced stages of deformation. He also indicated that the decrease in fracturing might be related to the fact that grains in the gouge matrix reached their "grinding limit", defined as the critical grain size at which grain fragmentation ceases [Kendall, 1978; Prasher, 1987; An and Sammis, 1994; Michibayashi, 1996; Hattori and Yamamoto, 1999]. Tsoungui et al. [1999] suggested a possible explanation of the above-mentioned "cushioning effect" invoked by Cladouhos, which might be related to a reduction in the deviatoric stress inside large grains surrounded with smaller grains, which, in turn, causes a hydrostatic effect and inhibits grain breakage.

Stress concentrations in granular materials have been studied with numerical models and with laboratory analogs, including two-dimensional photomechanical models, sandstone discs, glass beads, and quartz grains [e.g. Gallagher et al., 1974; Mandl et al., 1977; Cundall and Strack, 1979; Sammis et al. 1987; Biegel et al., 1989; Sammis and Steacy, 1994; Mueth et al., 1998; Aharanov and Sparks, 1999; Cates et al., 1999; Morgan and Boettcher, 1999b; Åström et al., 2000; Buchholtz et al., 2000]. These studies show that stresses applied to granular materials are not homogeneously distributed through the system. Subsets of grain contacts, known as "grain bridges" or "force chains", bear much higher than average contact forces, and transmit most of the stresses, while other grains remain relatively stress-free. If several different orientations of force chains are present, they form a network or "granular skeleton" [Cates et al.,

1999; Åström et al., 2000]. Gallagher et al. [1974] pointed out that micro fracturing (mostly extensional) occurred in grains along force chains and was related to the orientations and magnitude of the load applied, the packing, the sorting, and the grain shapes in the aggregate. Buchholtz et al. [2000] applied the Discrete Element Method (DEM) [Cundall and Strack, 1979; Rapaport, 1997] to simulate comminution in ball mills and showed that the more highly stressed grains in force chains are more likely to break. Several other authors [Engelder, 1974; Sammis et al., 1986; Sammis et al., 1987; Biegel et al., 1989; Marone and Scholz, 1989; Sammis and Steacy, 1994; Michibayashi, 1996; Hattori and Yamamoto, 1999; Blenkinsop and Fernandes, 2000] also noted that extensional microfractures in grains of both natural and experimentally deformed gouges are parallel to the direction of the inferred or applied maximum compression. Sparks and Aharonov (submitted to press, 2000) emphasized the role of the relatively low-stressed grains between force chains with regards to the life of the chains. They observed that new force chains take over old chains following the mobilization of "island grains" between the chains.

Remarkably interesting is also the role of PSD and its evolution with respect to the mechanical behavior of faults. Several authors [Sammis et al., 1986; Sammis et al., 1987; Sammis and Biegel, 1989; Biegel et al., 1989; Marone and Scholz, 1989; Blenkinsop, 1991; An and Sammis, 1994; Blenkinsop and Fernandes, 2000] have shown that the PSD in natural and experimentally deformed gouges follows a power law (fractal) distribution with different fractal dimensions [see Blenkinsop, 1991 for a summary of literature values]. Biegel et al. [1989] observed in their experiments that

gouges, which had an initial non-fractal PSD, evolved to a fractal distribution. Morgan [1999a] and Morgan and Boettcher [1999b] explored in detail the influence of fractal dimension on the mechanical behavior of fault gouge. In their numerical simulations they sheared layers of circular discs with self-similar size distributions. Grains were not allowed to break; hence, inter-grain slip and rolling were the only possible deformation mechanisms. They observed that the strain was accommodated by localized slip surfaces at 10°-15° from shear boundaries, at 70°-110° from shear boundaries, and parallel to shear boundaries.

Åström and Herrmann [1998] employed MD to simulate fragmentation of elastic circular discs. They used two different breaking criteria based on the total compression on a grain and on the largest force at the contacts between grains and showed that the evolution of the PSD greatly depends on the breaking criterion adopted. Tsoungui et al. [1999] simulated grain breakage in a two-dimensional pack of circular disc-shaped grains under uniaxial compression and compared the results with laboratory experiments performed on a similar aggregate of molding plaster discs. They observed that "large grains surrounded by small grains cannot break despite the increase of the external pressure", because of the "hydrostatic effect" created by small grains. Furthermore, they showed that in both numerical simulations and experiments at the beginning of compression the frequency of breakage events linearly increases with the applied pressure, but beyond a certain value $P_{sat}$, the frequency tends to reach a plateau. Their interpretation of this phenomenon is that the system reaches "saturation" when larger grains are completely surrounded by smaller grains.

Aharonov and Sparks [1999] and Sparks and Aharonov (submitted to press, 2000) employed also the MD method to simulate two-dimensional layers of circular discs of different diameters under variable systems of assigned shear and normal forces. In these experiments, grains were not allowed to break, such that grain sliding and rolling were the only active deformation mechanisms. They showed, among other things, that the orientation and stress state on grain contacts evolve over time and may be critical to triggering localization and instabilities.

Many questions about the evolution of granular systems remain unanswered. For instance, can we test in some way the "constrained comminution" model of Sammis et al. [1987]? Why certain large grains survive cataclasis and others don't? What are the processes that lead to the preservation of large grains in fault gouges? What type of evolution in grain breakage can we expect within a fault gouge? Is there some critical stress for which comminution starts to occur? How does the particle size distribution in a fault gouge evolve with depth? What are the effects of such evolution on friction? These are some of the questions addressed in this thesis by using numerical models based on fundamental principles of mechanics.

# METHODS

## Distinct Element Method

Granular materials are defined as systems of distinct grains moving independently from one another and interacting only at contact points. These materials can be studied by using the Distinct Element Method (DEM) [Cundall and Strack, 1979]. This numerical technique is an explicit scheme, which calculates interaction forces between grains for each grain-grain contact, and the resulting motion of each grain. The force between a pair of grains at a given time depends only on the relative positions and velocities of those grains. Whenever any two grains interact, they overlap by a small fraction of their radii and visco-elastic forces represent the interaction. At every time step the method applies Newton's second law (1), such that position, linear velocity, and angular rotation of every grain can be calculated from the sum of the forces acting at the contact points.

$$\sum_i \vec{F}_i = m\vec{a} \qquad (1)$$

Commonly, the DEM is used to simulate systems of two-dimensional circular disks or three-dimensional spheres, but it could be applied to grains of any shape as well. Liquids and powders are often studied by means of DEM [e.g. Cundall and Strack, 1979; Donzé et al. 1994; Rapaport, 1997; Aharonov and Sparks, 1999; Granick, 1999; Morgan, 1999a; Morgan and Boettcher, 1999b; Tsoungui et al, 1999; Åström et al., 2000; Buchholtz et al., 2000].

The goal of this research project was to develop an understanding of how grain breakage evolves in a shearing granular system and how it affects the stress distribution and dynamics of the system. To achieve this, it required developing new subroutines for an existing DEM code GranFrixl [Aharonov and Sparks, 1999; Sparks and Aharonov (submitted to press, 2000)]. To emphasize the importance of such a development, the main characteristics of the original version of GranFrixl before the introduction of the new subroutines are described in the next subsection.

*Simulating granular materials with the original version of GranFrixl*

GranFrixl is a code written in FORTRAN 77 [Aharonov and Sparks, 1999], which simulates the behavior of a system of non-cohesive, two-dimensional circular disks. Top and bottom boundaries of the system are made of two arrays of cemented rigid half-disks of different sizes, such that they simulate rough walls and are subjected to normal and shear stresses. The system is periodic in the horizontal direction, which implies that if a grain leaves the system from the right side, it immediately reenters the system from the left side and also those grains at one boundary interact directly with grains of the opposite boundary. Because of this wraparound effect [Rapaport, 1997] the system simulates an infinite layer of grains.

Two grains of radii $R_i$ and $R_j$ interact when the distance between their centers, $R_{ij}$, is

$$R_{ij} < R_i + R_j \qquad (2)$$

and the two grains overlap by $\varepsilon$

$$\varepsilon = R_i + R_j - R_{ij} \qquad (3)$$

This overlap creates an elastic resisting force.

In order to not excessively violate conservation of mass, the elastic parameters of the problem are chosen so that overlaps are small, typically < 1% of a grain radius.

Normal and shear visco-elastic forces exist at the contact for the duration of the interaction. Normal contact forces are modeled by a linear coil spring and a viscous dashpot acting in parallel between the centers of the two grains (Figure 1) and represented by

$$\vec{F}_{ij}^{n} = \left[k_n \varepsilon - \gamma m_{ij} \left(\vec{V}_{ij} \bullet \hat{n}\right)\right]\hat{n} \qquad (4)$$

where $k_n$ is the normal spring constant, $\gamma$ is a damping coefficient, $m_{ij}$ represents the harmonic mean of the masses of the two grains, $\vec{V}_{ij}$ is the relative velocity vector between the two grains, and $\hat{n}$ represents the unit vector normal to the contact surface.

The contact shear forces are modeled by a leaf spring, which is displaced by the shear motion of the grains (Figure 2) and are represented by

$$\vec{F}_{ij}^{s} = \left\{\min \left[k_s \Delta S, \mu \vec{F}_{ij}^{n}\right]\right\}\hat{s} \qquad (5)$$

where $k_s$ is the shear spring constant, $\Delta S$ is the shear displacement of the leaf spring since the initial contact, $\mu$ is the surface friction coefficient, and $\hat{s}$ is the unit vector in the tangential direction. With increasing shear displacement along the contact, $F_{ij}^{s}$ increases until it reaches a maximum, defined as the frictional sliding limit.

In the densely packed granular systems investigated here, the forces on grains are nearly at static equilibrium so that grain accelerations are very small.

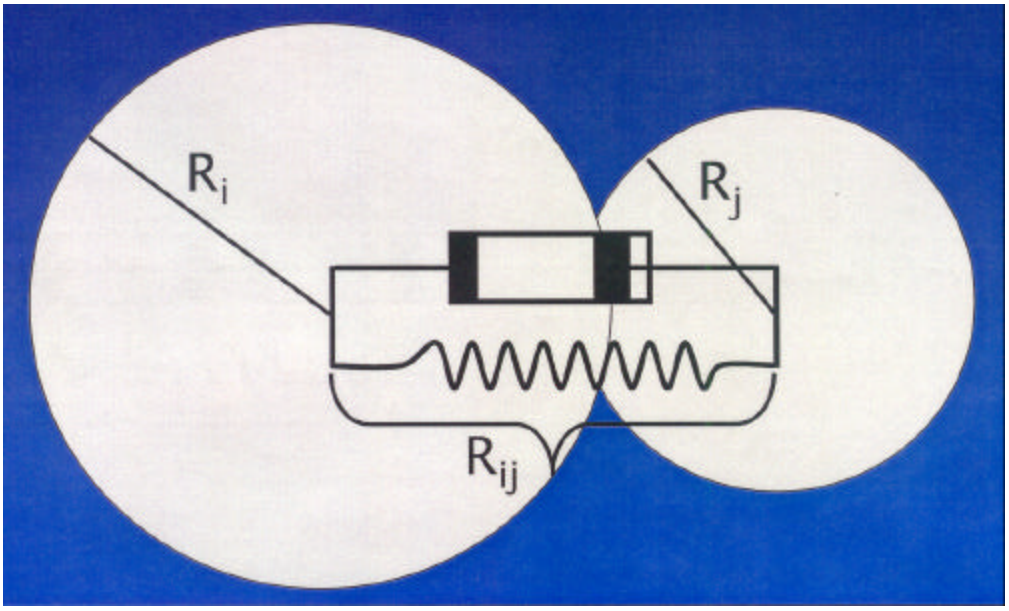


**Figure 1. Model of normal force at grain contact.** Visco-elastic forces normal to the grain contact are modeled by a spring and a dashpot arranged in parallel between the centers of the two contacting grains of diameters $R_i$ and $R_j$. $R_{ij}$ is the distance between the centers during the interaction.

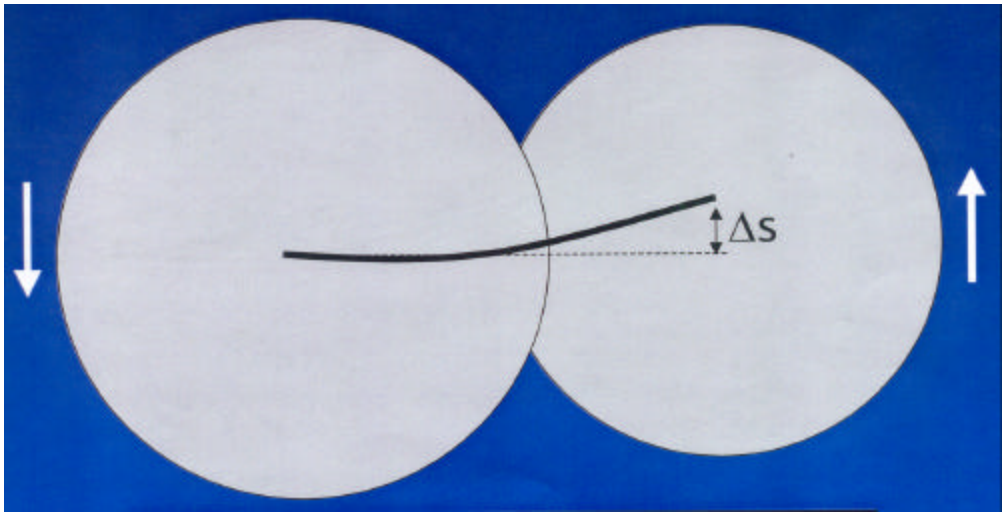


**Figure 2. Model of shear force at grain contact.** Shear forces are modeled by a leaf spring (continuous black line) displaced by ΔS. When a critical displacement (proportional to the normal force) is reached, the grain may continue to slide frictionally, without further increasing the resistance.

In order to obtain the grain position, linear and angular velocities, the above-described forces are integrated through time by using a numerical scheme based on the Verlet algorithm [Rapaport, 1997], a leapfrog scheme, in which position and velocity of a grain are calculated at two slightly different times. For accuracy and stability of the numerical simulations, the time step is kept to a small fraction ($\approx 0.1$) of the travel time of a compressional elastic wave through the smallest grain. If a grain breaks and the radius of a newly-formed grain, $r_{new}$ (equation 13) is smaller than the prior minimum radius $r_{small}$=min (radius (i)), then the time step dt is reset to

$$dt = dt \cdot \sqrt[3]{\left( \frac{r_{new}}{r_{small}} \right)^2} \qquad (6)$$

At any time, the positions, velocities, and forces on all grains are calculated, as well as bulk properties including porosity and the average tractions acting on the walls.

In the original version of GranFrixl grains were not breakable. Therefore, the only deformation mechanisms allowed were grain slipping and grain rotation. Although these are fundamental mechanisms, the important process of grain comminution is not modeled. The comminution process and how it was implemented in GranFrixl is the topic discussed in the next section.

**Incorporating Grain Breakage in GranFrixl**

When one considers the phenomena of grain breakage, it is necessary to choose a criterion that describes the conditions under which breakage occurs. Moreover, one also needs to define the way grains break (i.e. the "mode" of breakage). The rest of this chapter describes the non-dimensional variables used, the breakage criterion employed, the initial configuration of the newly formed fragments after breakage, and the adopted breakage limit. The full text of the subroutines devised is shown in the Appendix.

*Non-dimensional variables*

The equations of motion solved by GranFrixl are non-dimensionalized by the following set of scaling factors for length ( $X_0$ ), stress ($\sigma_0$), force ( $F_0$ ), time ( $T_0$ ),and velocity ( $V_0$ ).

$$
\begin{aligned}
X_0 &= \overline{D} \\
\sigma_0 &= E \\
F_0 &= EX_0^2 \\
T_0 &= \sqrt{\frac{\overline{m}}{E\overline{D}}} \\
V_0 &= \frac{X_0}{T_0}
\end{aligned}
\qquad (7)
$$

where $\overline{D}$ is the average diameter of the initial system and $\overline{m}$ is the mass (equivalent to area in 2-D) of a grain of diameter $\overline{D}$. The time scale, $T_0$, represents the travel time of elastic waves through the grain of average size. Since no body force is acting in the

system, the choice of the scaling factor for forces, $F_0$, is determined only by the stiffness and the size of the average grain. Finally, the stress scaling factor, $\sigma_0$, is equal to the Young's Modulus, E, of the grain material.

*Grain breakage criterion*

The simplest criterion for grain breakage is to compare the instantaneous state of stress in the grain with some measure of the strength of the grain. In the present research, two different criteria were explored and ultimately only one was adopted for all the simulations. In the remainder of this section, the tested breakage criteria will be described.

The first criterion consisted in using the value of the total force on a grain [Åström and Herrmann, 1998] and compares it against the pre-defined grain strength. But, such criterion was eventually dismissed, because it produced an unrealistic cascading grain breakage process in the whole system.

The breakage criterion used is similar to the one Tsoungui et al. [1999] adopted, and takes into account the common observation that intra-granular fractures in fault gouge materials are mostly extensional. In this model, a grain will break if it has an internal tensional stress greater than the assigned grain strength.

For a grain in force-balance equilibrium, such that it is not undergoing linear or rotational accelerations, the stress field within the grain can be calculated directly from the contact forces (as is described in the next subsection). In practice, the stress tensor at the center of each grain was used as a proxy for the stress state inside the whole grain,

since that is the location where we would expect the highest tension to occur (Figure 3) [Tsoungui et al., 1999]. The magnitude of the maximum tensional (tension positive) stress $\sigma_i^{max}$ was compared to the assigned tensional strength $T_i$ (equation 12) in each grain, creating a breaking index, $\delta$ given by (8)

$$\delta_{i^{\oplus}} = \sigma_{i^{\oplus}}^{max} - T_{i^{\oplus}} > 0 \qquad (8)$$

Breakage occurs for the grain $i^{\oplus}$ that has the largest positive breaking index $\delta_{i^{\oplus}}$ in the system.

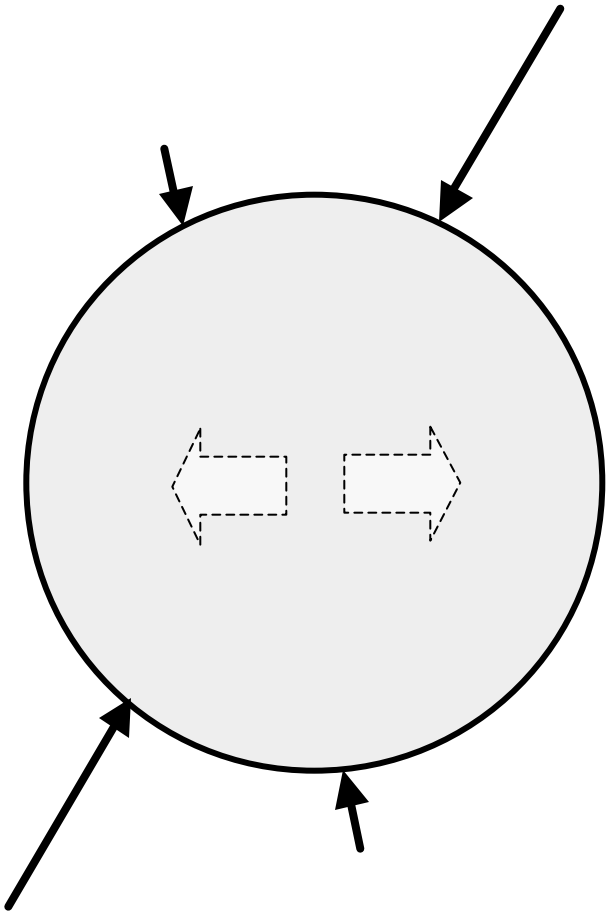

**Figure 3. Tension may be generated at the center of the grain**. A balanced system of compressional boundary forces (black arrows) applied to a grain boundary may generate tension (dashed large arrows) at the center of the grain.

*Stress state inside of grains*

The description in this subsection is based on the solution of Muskhelishvili [1963]. The solution provides the stress field within the grain for a balanced system of concentrated boundary forces. But, as described above, the stress state, represented by (9), is only calculated at the center of the circular grains, where the maximum tensile stresses are expected.

$$\bar{\bar{\sigma}} = \begin{pmatrix} \sigma_{xx} & \sigma_{xy} \\ \sigma_{yx} & \sigma_{yy} \end{pmatrix} \qquad (9)$$

The elastic stress field utilizes superposition of the effects of a system of boundary forces. The contributions of the $k^{th}$ boundary force to the stress components are

$$\sigma_{yy}^{k} = \frac{S_1^k + S_2^k}{2}$$

$$\sigma_{xx}^{k} = \frac{S_1^k - S_2^k}{2} \qquad (10)$$

$$\sigma_{xy}^{k} = \sigma_{yx}^{k} = \frac{S_3^k}{2}$$

with (refer to Figure 4 for symbols)

$$S_1^k = \frac{X_k \cos \alpha_k + Y_k \sin \alpha_k}{\pi R}$$

$$S_2^k = -\frac{X_k (\cos \alpha_k + \cos 3\alpha_k) + Y_k (\sin 3\alpha_k - \sin \alpha_k)}{\pi R} \qquad (11)$$

$$S_3^k = \frac{X_k (\sin \alpha_k + \sin 3\alpha_k) + Y_k (\cos \alpha_k - \cos 3\alpha_k)}{\pi R}$$

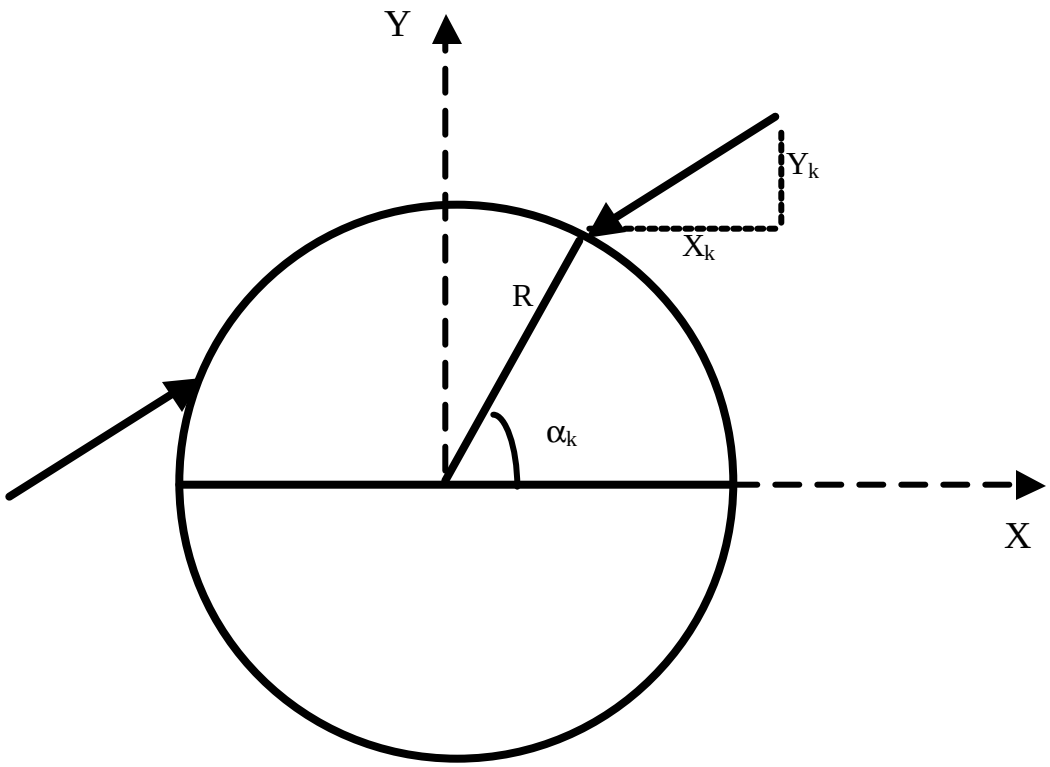


**Figure 4. System of balanced concentrated forces applied to a circular boundary.** A balanced system of boundary forces applied to a circular grain boundary. Note that because of frictional shear forces, the two forces don't have to lie necessarily on the same chord. After Muskhelishvili [1963].

$X_k$ and $Y_k$ are the x-component and y-component, respectively, of the $k^{th}$ applied force and $\alpha_k$ represents the angle of the applied force, measured counterclockwise from the positive x-direction, and $R$ is the radius of the disk. Once the stress tensor for a grain is found, the eigenvalues are calculated to determine the principal stress components. The largest positive eigenvalue of a grain i is the $\sigma_i^{max}$ of equation (8).

*Size dependence of grain strength*

Different tensional strengths $T_i$ were assigned to different grains according to the following functional relation

$$T_i = T^*\left(1+\frac{1}{D_i}\right) \qquad (12)$$

where $D_i$ is the diameter of grain i and $T^*$ represents one-half of the strength of a grain of diameter one (i.e. average grain in the system). According to Gallagher's [1976] data, the tensile strength of a 1 mm quartz grain under diametrical compression is around 35 MPa corresponding to a non-dimensional $T^*$ of $4.0 \times 10^{-4}$. This tensile strength is then compared to the maximum tensile stress within each grain.

*Configuration of fragments after breakage*

When a grain exceeds the breakage criterion, it is replaced at the next time step by a set of seven identical smaller circular grains of radii $r_{new}$ (13). The approximation of circular grains breaking into smaller circular grains is a limitation of this study that leads

to some artifacts (discussed below). Our primary justification for this approximation is the simplicity of algorithms that use circular grains. An alternative approach that also takes advantage of circular grains is to build grains out of several circular sub-grains bonded by attractive forces to each other [Donzé et al., 1994; Granick, 1999; Place & Mora, 2000]. However, in order to realistically approach the large range of grain sizes in comminuted material, each composite grain would have to originate from many circular grains, greatly increasing the computational expense.

The set of seven new grains is initially arranged in hexagonal packing (Figure 5). Occasionally this packing will create larger forces (overlaps) than existed in the original grain. In order to find a configuration that minimizes contact forces the following procedure, suggested by Peter Cundall (personal communication, 2000) is implemented. The normal time stepping procedure is paused and the positions of all the grains in the system held constant, except for the newly formed grains. These new grains rearrange themselves in order to establish the optimal configuration with minimum overlap with neighboring grains (Figure 6). This approach uses the same algorithm for calculating forces and velocities as the normal time stepping, except only the new grains are allowed to move. The code then resumes its regular flow.

For some breakage events, the rearrangement procedure described above does not eliminate all contact forces on the new grains. In fact, the resulting forces may be large enough to cause a cascade of breakage events of surrounding grains. Since their behavior is most likely an unphysical result of the circular grain model, further steps are taken to suppress large forces in the area of the new grains.

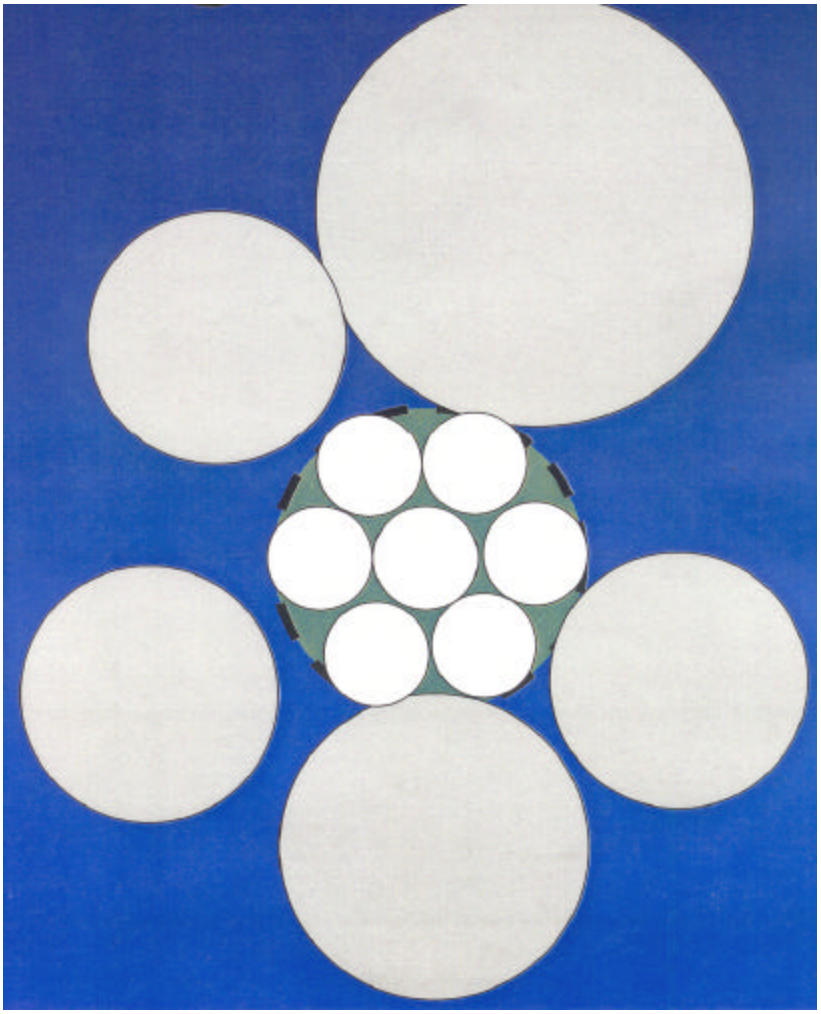

**Figure 5. Initial grain arrangement after breakage.** When a grain fails (green grain), it is instantaneously replaced by a set of seven smaller circular grains initially arranged in hexagonal packing.

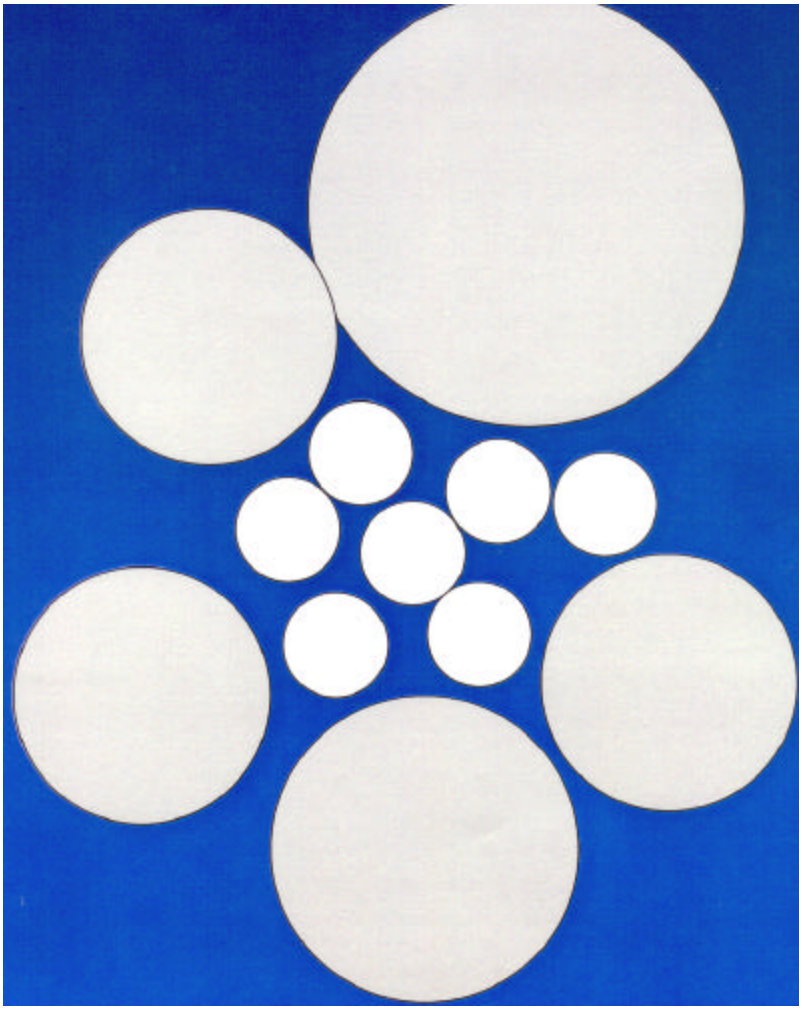

**Figure 6. Newly formed grains after rearrangement.** Newly formed grains are allowed to rearrange in available pore space to find a configuration with minimum overlap with neighboring grains.

It is assumed that the total area of the seven new grains accounts for 92 % of the area of the original grain so that

$$r_{new} = \sqrt{\frac{0.92}{7.0}} R_{i\oplus} \qquad (13)$$

while the remaining 8 % is finely pulverized and dispersed in the pores, and cannot be tracked thereafter. This assumption is justified by fragmentation of grains into few large pieces, perhaps angular, and many small pieces. Note that if the code were to track the position of these small pieces, they would be filling the pore space. So the observed compaction is correct, but the calculated porosity is an upper bound, it would actually be lower.

Finally, the instantaneous replacement of a grain can lead to a short period of unbalanced forces on the neighboring grains. To prevent these neighboring grains from breaking during this transient state, the breakage process is halted for a short dimensionless time of 200 to allow the system to begin to equilibrate to the new configuration of grains.

*Breakage limit*

Steir and Schönert [1972] performed a series of experiments in which they observed fracture patterns in single quartz and limestone grains subjected to diametrical compression. Grains larger than 5 μm failed by cracking along a number of radial fractures. Smaller grains displayed some degree of plastic deformation, while grains with diameters of about 1 μm displayed pervasive plastic deformation. A transition to a

different deformation mechanism at small grain sizes has led to the idea of a "comminution limit" below which grain fracture does not occur (see Prasher [1987] for a review of the topic).

In this numerical model, the computational expense increases non-linearly with the amount of breakage, due to the increasing number of grains and the reduction in time step. For practical reasons, it was necessary to set a lower limit on the grain size by prescribing a scaled grain diameter $d_c$, below which breakage is not allowed.

Various breakage limits, $d_c$ (0.0017, 0.07, 0.14, and 0.28 of the initial average grain diameter), were tested on the same initial set of grains. The systems with different $d_c$ behaved exactly in the same manner up to a certain point in the runs (depending on the particular value of $d_c$). Subsequently, the different runs diverged from each other and followed different evolutions, which demonstrates a strong sensitivity to the breakage limit values. For all the runs described in the next chapter a high critical limit value of $d_c$= 0.28 were employed. Such choice was dictated mainly by the marked decrease in allowable time step of the code with decreasing grain size thereby increasing the run time significantly. This limitation calls for future improvements in the current version of the code.

*Set-up of shear experiments*

A system of grains was confined between two rigid plates by an applied normal stress. Eight grains bonded together along their centers create each rough wall. The system was periodic in the direction parallel to the plates, with a non-dimensional

wavelength of 8. Because of this periodicity, the applied normal stress on the walls creates an internal stress state that is hydrostatic. So this applied stress, N, is equivalent to a confining pressure. One wall is allowed to adjust freely to maintain a constant average normal stress, and as a result the system can dilate and compact.

One wall is also moved at a constant velocity ($3.0x10^{-4}$) parallel to the layer, to generate shear.

# RESULTS AND DISCUSSION

## Matrix of Numerical Simulations

Five numerical experiments were performed to specifically determine the effects of different confining pressures (i.e. depths) on the rates of grain breakage and the evolution of PSD with displacement in simulated fault gouges.

The initial system of grains was identical for all the runs (Figure 7) and consisted of 74 grains with dimensionless diameters randomly chosen from a pre-defined Gaussian distribution that had a mean of 1.0, standard deviation of 0.5, and was clipped at 0.5 and 1.5. From this distribution a subset of 58 grains (Figure 8) contained between the rigid top and bottom boundaries, made out of eight grains each, were allowed to break.

The initial grain assembly was pre-compacted at a prescribed confining pressure without allowing for grain breakage. Subsequently, the confining pressure was held constant and the top wall was displaced laterally with a constant non-dimensional shear velocity of $3.0 \times 10^{-4}$ such that the simulated fault displayed a right-lateral motion. Since the shear velocity was constant and identical for all the runs, time is directly proportional to displacement.

After onset of shearing motion, grain breakage was allowed. For all five runs, grains of diameter 1.0 were assigned a dimensionless $T^*$ (one-half of the tensional strength) of $4.0 \times 10^{-4}$ and the breakage limit was chosen to be 0.28.

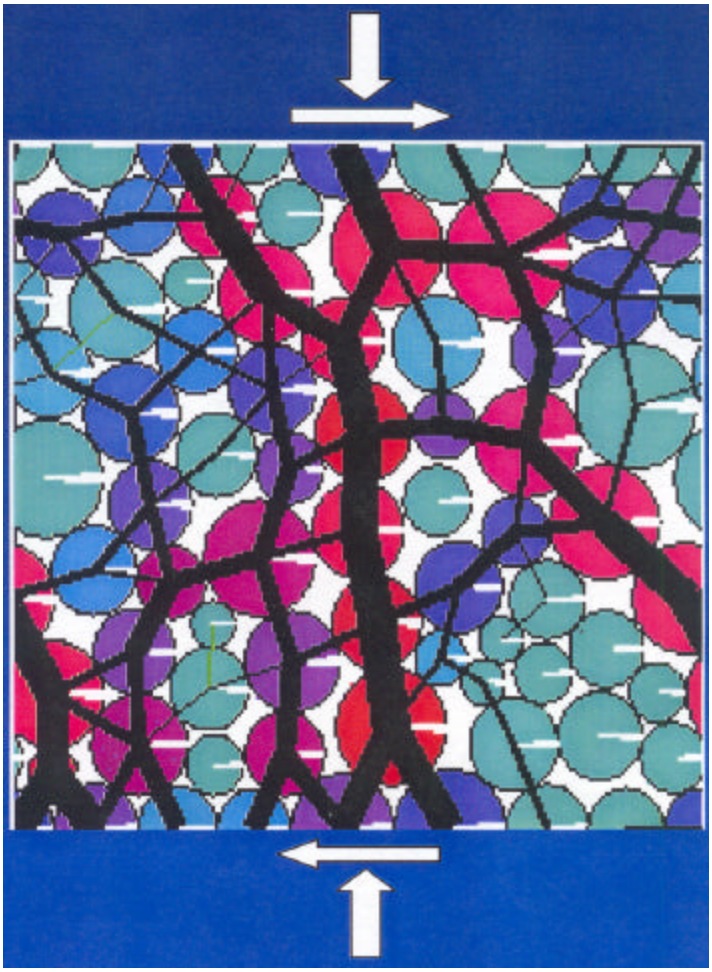

**Figure 7. Initial system.** Initial system of 74 grains subjected to normal and shear forces (white arrows). Left and right boundaries are periodic. Grains in red are subjected to large compressive forces, while grains colored in light blue have no contact forces. The black lines represent the relative magnitude and direction of the contact forces between the grains (the thicker the lines, the larger the force). The forces represented here are prior to the onset of shearing.

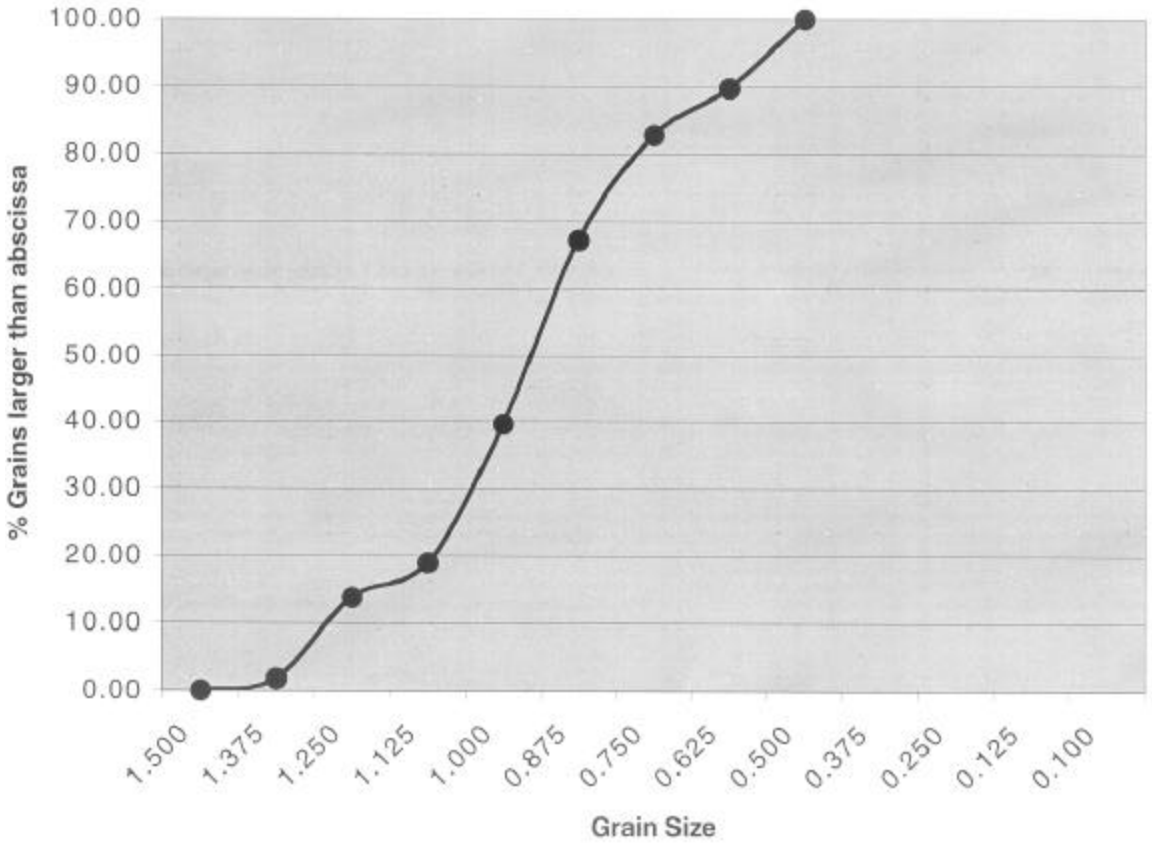


**Figure 8. Initial grain size distribution of the subset of 58 breakable grains.**

Frequency curve showing the distribution of the subset of the 58 “breakable” grains contained between top and bottom walls.

The only parameter that varied from run to run was the confining pressure, N. Therefore, the value of R defined as the ratio between $T^*$ and the N can describe the five numerical simulations

$$R = \frac{T^*}{N} = \frac{4.0 \cdot 10^{-4}}{N} \qquad (14)$$

The range of R values explored (Table 1) was small, but enough to cause significant differences in the amount of breakage.

**Table 1.** Matrix of numerical runs

| RUN | RATIO R | N |
|---|---|---|
| **R1.3** | 1.3 | $3.0 \times 10^{-4}$ |
| **R2.0** | 2.0 | $2.0 \times 10^{-4}$ |
| **R4.0** | 4.0 | $1.0 \times 10^{-4}$ |
| **R6.0** | 6.0 | $6.7 \times 10^{-5}$ |
| **R8.0** | 8.0 | $5.0 \times 10^{-5}$ |

## Results

The following five sub-sections report the main findings obtained from the numerical simulations relevant to the goals set for this research project. The grain breakage evolution, the particle size distribution evolution, the porosity evolution, and the frictional properties of each run listed in Table 1 will be described. The spatial distribution of breakage will also be illustrated for run R2.0.

### *Grain breakage evolution*

One fundamental observation for all the runs was that the grains that failed were always within prominent force chains and typically subjected to only a few large contact forces. Only in such grains is there sufficient tensional stress to overcome the grain strengths. Grains subjected to numerous contact forces were characterized by near hydrostatic internal stress, and therefore, they do not reach the tensile limit.

One measure of the extent of breakage is the cumulative number of breakage events (CBE) shown in Figures 9 and 10. The near linearity of the breakage events curves for runs R1.3 and R2.0 in the semi-logarithmic plot (Figure 10) suggested a logarithmic dependence of breakage on displacement. An attempt was made to fit (Table 2) the breakage curve for each run with a logarithmic function shown as thin lines in Figure 9 and of the type

$$\mathrm{CBE} = \mathrm{A} + \mathrm{B}\ln\left(l\right) \qquad (15)$$

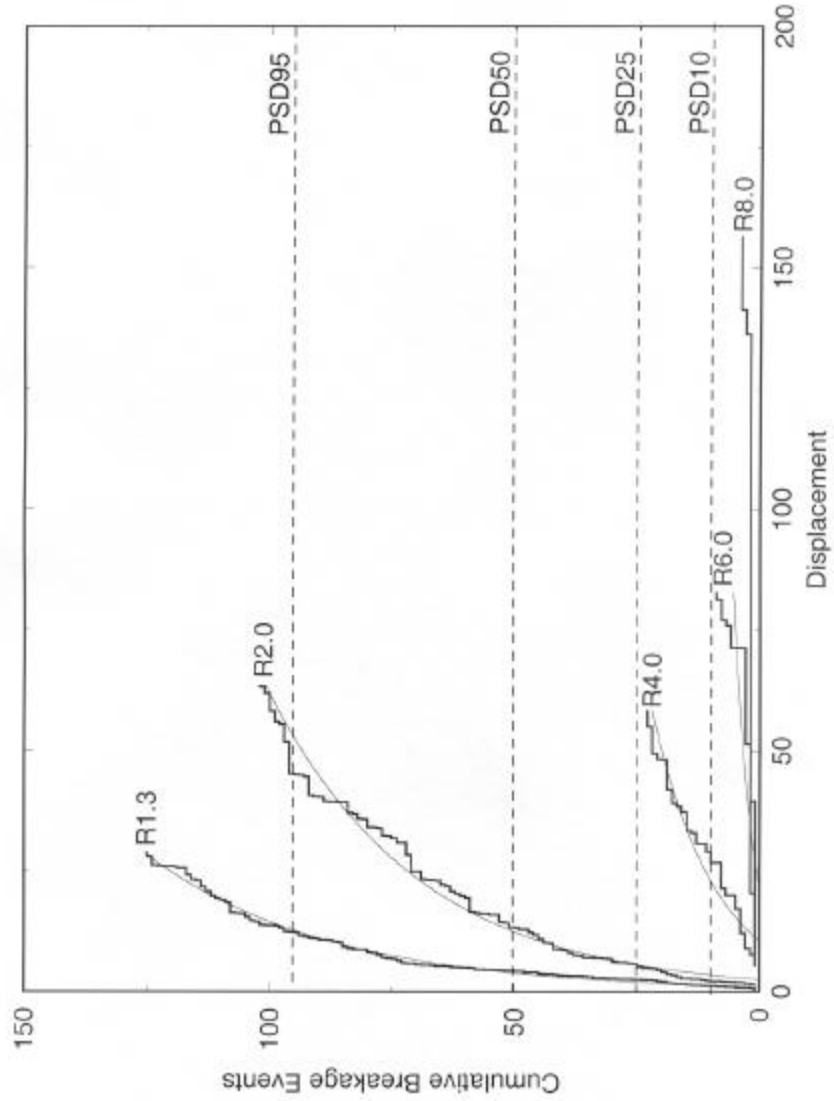


**Figure 9. Grain breakage evolution.** Plot of the cumulative breakage events (CBE) vs. displacement for all the runs (thick jagged curves) fitted by logarithmic curves (thin continuous curves). The dashed lines indicate arbitrary levels of breakage, at which particle size distributions are compared.

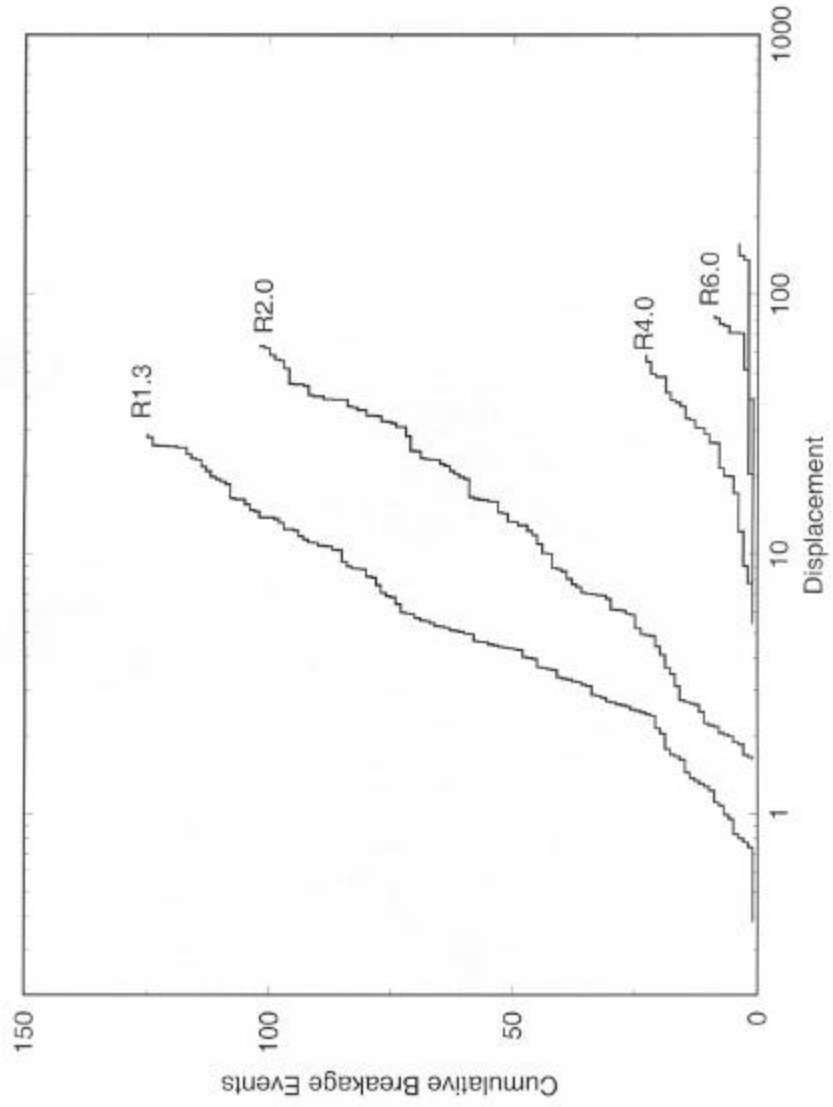


**Figure 10. Cumulative breakage events vs. displacement on semi-logarithmic plot.** Same plot as Figure 10 on semi-logarithmic scale showing the linear relation between CBE and logarithm of displacement.

where $l$ is the displacement along the fault. A reasonably good fit was obtained for the three runs with significant breakage, but the two runs (R6.0 and R8.0) do not follow well the relationship.

**Table 2.** Logarithmic regression coefficients of CBE-displacement curves of Figure 9

| RUN | A | B | CORR. COEFF. |
|---|---|---|---|
| **R1.3** | -172.98 | 37.56 | 0.99 |
| **R2.0** | -172.38 | 31.26 | 0.99 |
| **R4.0** | -89.85 | 12.92 | 0.96 |
| **R6.0** | -31.10 | 4.07 | 0.70 |
| **R8.0** | -6.53 | 0.99 | 0.75 |

Figure 9 shows that, as expected, the systems subjected to higher confining pressures will experience more breakage events for a given displacement. All the intergranular forces in the system scale with the confining pressure, so we expect the number of breakage events to scale with N too. Their relationship is shown in Figure 11, which plots CBE relative to the confining pressure for the runs with significant breakage (R1.3, R2.0, and R4.0) at different displacements ($\lambda$ equal to 3.0, 3.8, 4.5, 7.5, 15.0, 22.5, and 27.0). The limited data presented here appear to confirm that CBE at a given displacement is linearly related to N. The data for different displacements all point to a critical confining stress for significant breakage. The critical N value from Figure 11 corresponds to an R-value of about 5.0. Therefore, one would not expect much breakage

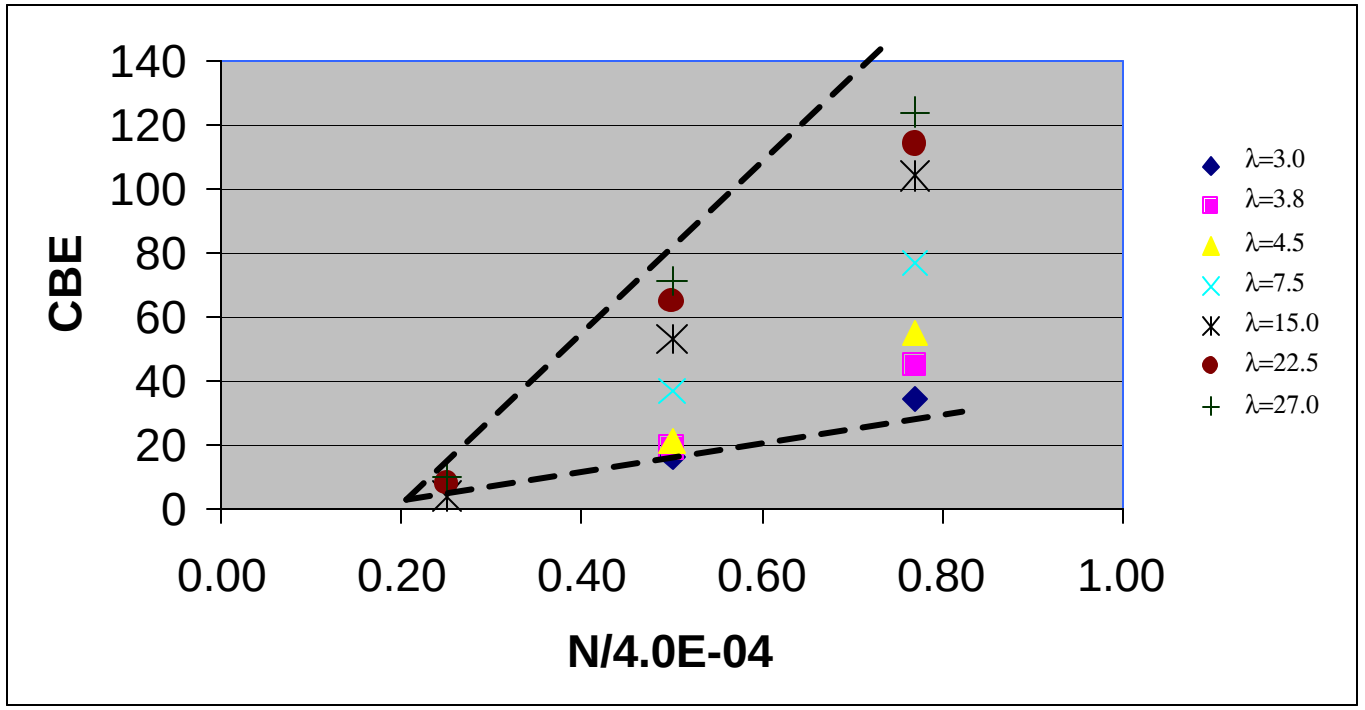


**Figure 11. Cumulative breakage events vs. confining pressure.** Plot of the Cumulative Breakage Events (CBE) with respect to the confining pressure (for runs R1.3, R2.0, and R4.0) at different displacements λ (3.0, 3.8, 4.5, 7.5, 15.0, 22.5, and 27.0). The dashed lines represent the linear envelopes of the data points

in the runs R6.0 and R8.0. The fact that some small amount of breakage does occur in these runs, that does not fit the relationships with N and displacement in Figures 9 and 10, indicates that even when the average conditions in the system are not favorable for grain breakage, transient packing and stress states can occur which occasionally break grains. This process has not been modeled here.

*PSD evolution*

The variations in PSD with displacement for the different runs were determined after a discrete number of breakage events (10, 25, 50, and 95 failed grains, shown by the dashed lines in Figure 9).

This approach allowed comparison of the different runs at the same degree of damage. The determinations of the PSDs were performed by grain count. The results are displayed in Figures 12, 13, 14, and 15 as cumulative frequency curves. In Figure 12, it can be noticed that the initial unimodal system (dashed line) of runs R1.3, R2.0, and R4.0 rapidly evolves to a multi-modal system after only 10 grains break.

As grain breakage continues the PSD are skewed to the smaller grain sizes. The most interesting feature of these plots is the strong similarity of the distributions at the same amount of damage, even though the systems were deformed to different displacements and under different stress conditions. The only independent control on these distributions appear to be the total damage, CBE which in turn depends on a combination of confining stress and displacement.

Grain breakage evolution and PSD evolution for run R2.0 are linked to each other in Figure 16, which represents the histograms of the number of grains that broke versus displacement versus their size. Referring to Figure 16, the initial phase of rapid breakage is indicated as "$\lambda < 2.4$", while the label "$\lambda > 2.4$" represents the subsequent phase of slower breakage rates. Notice that the sharp peak in the latter histogram associated with the 0.25-0.50 class is, at least to some extent, caused by the applied breakage limit of 0.28.

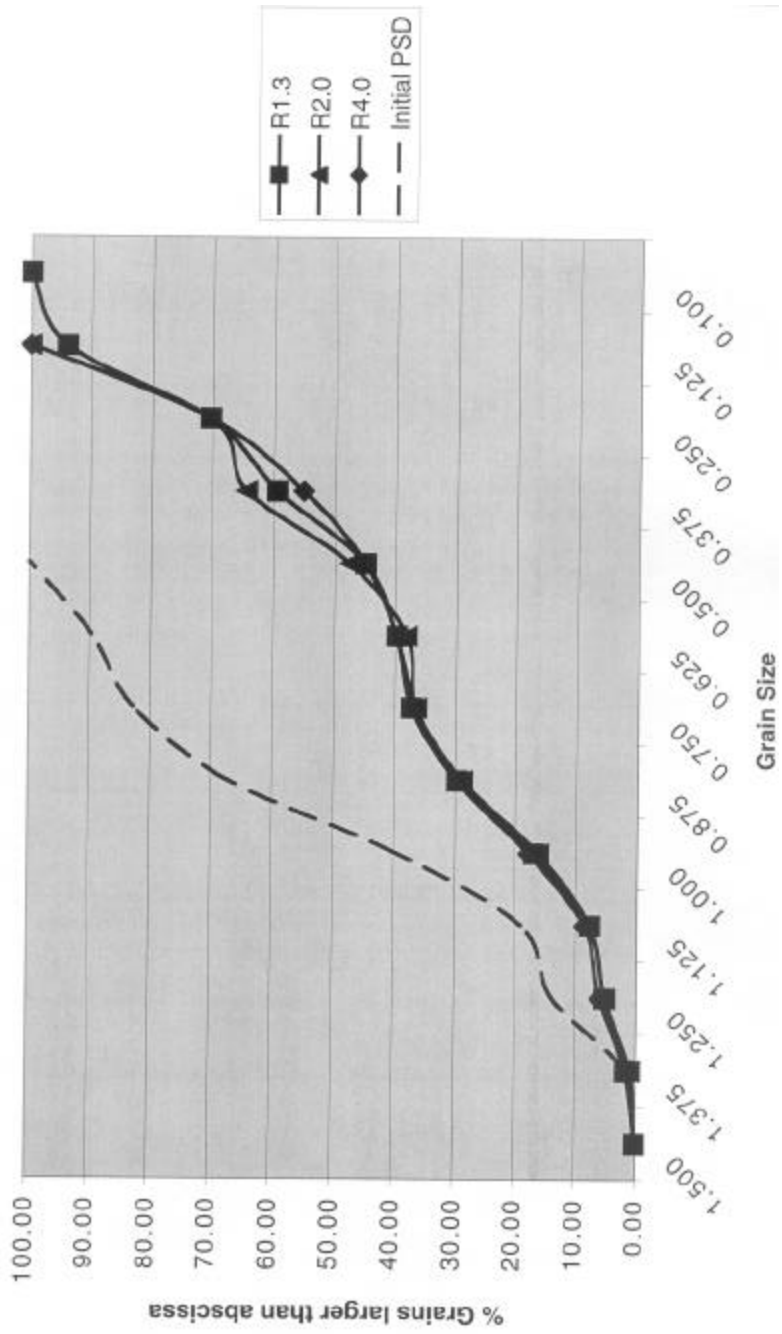


**Figure 12. PSD10.** Cumulative frequency PSD curves after only 10 grains broke (continuous lines). The dashed line represents the initial PSD.

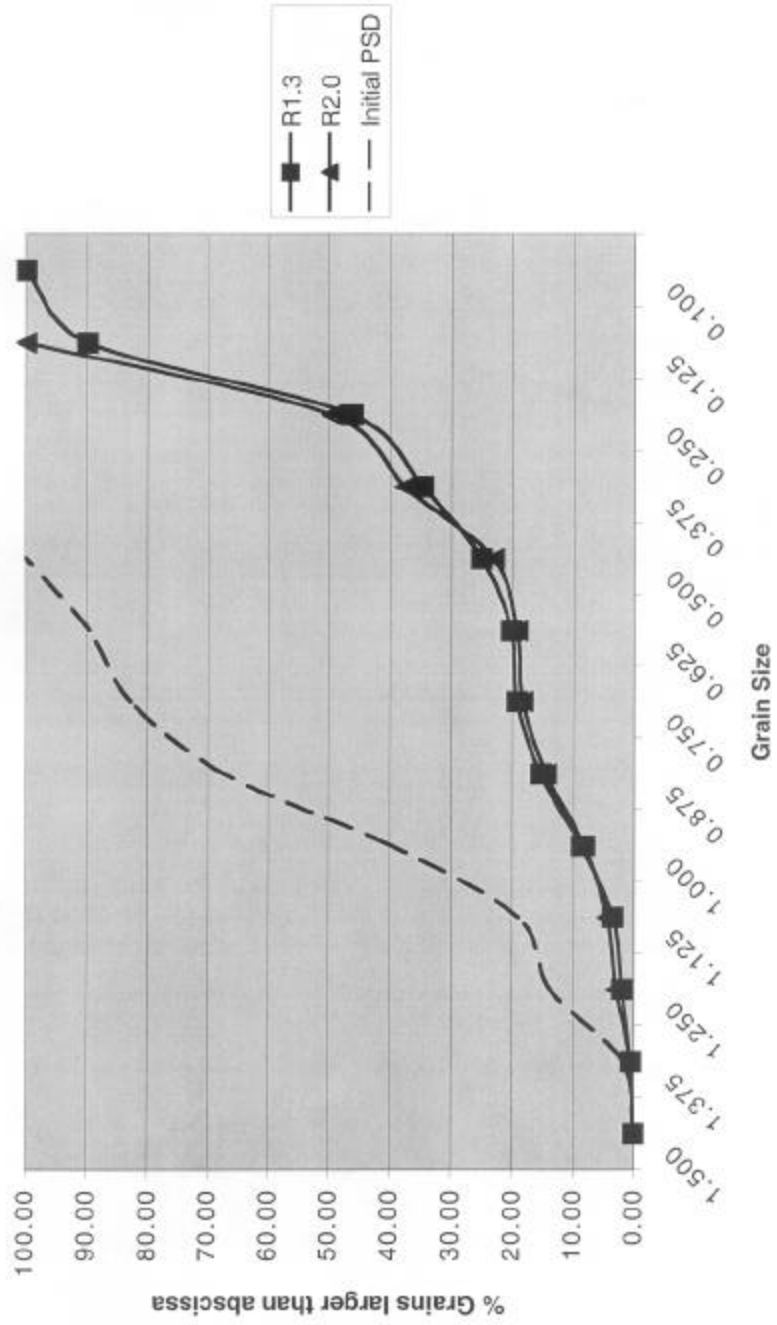


**Figure 13. PSD25.** Cumulative frequency PSD curves after only 25 grains broke (continuous lines). The dashed line represents the initial PSD.

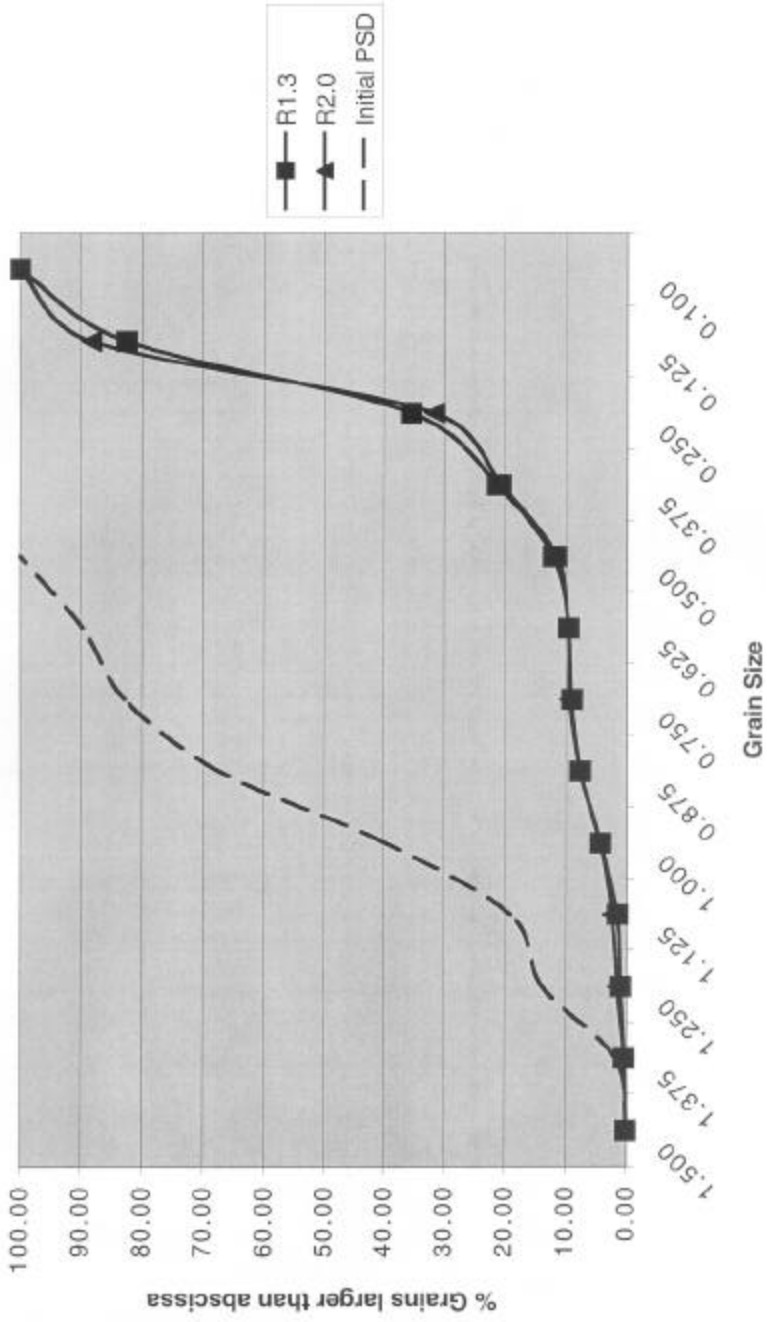


**Figure 14. PSD50.** Cumulative frequency PSD curves after only 50 grains broke (continuous lines). The dashed line represents the initial PSD.

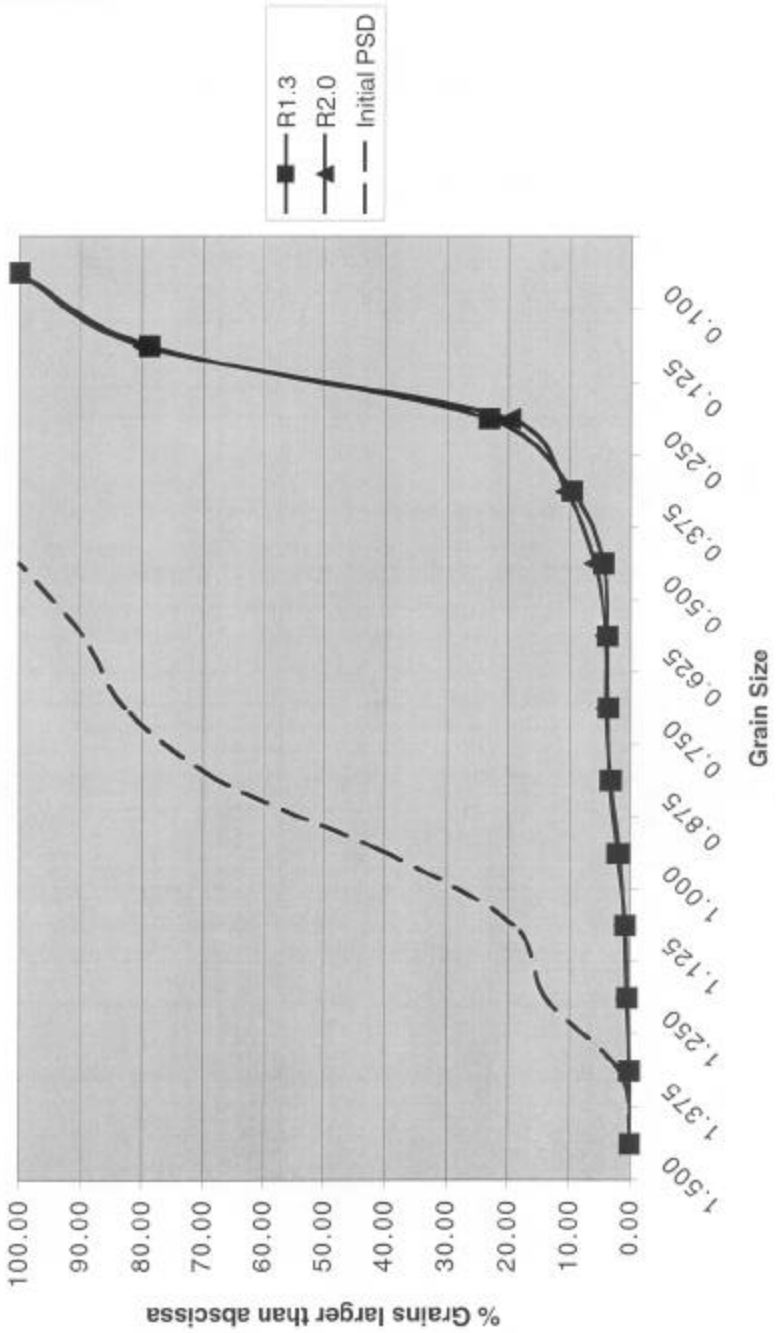


**Figure 15. PSD95.** Cumulative frequency PSD curves after only 95 grains broke (continuous lines). The dashed line represents the initial PSD.

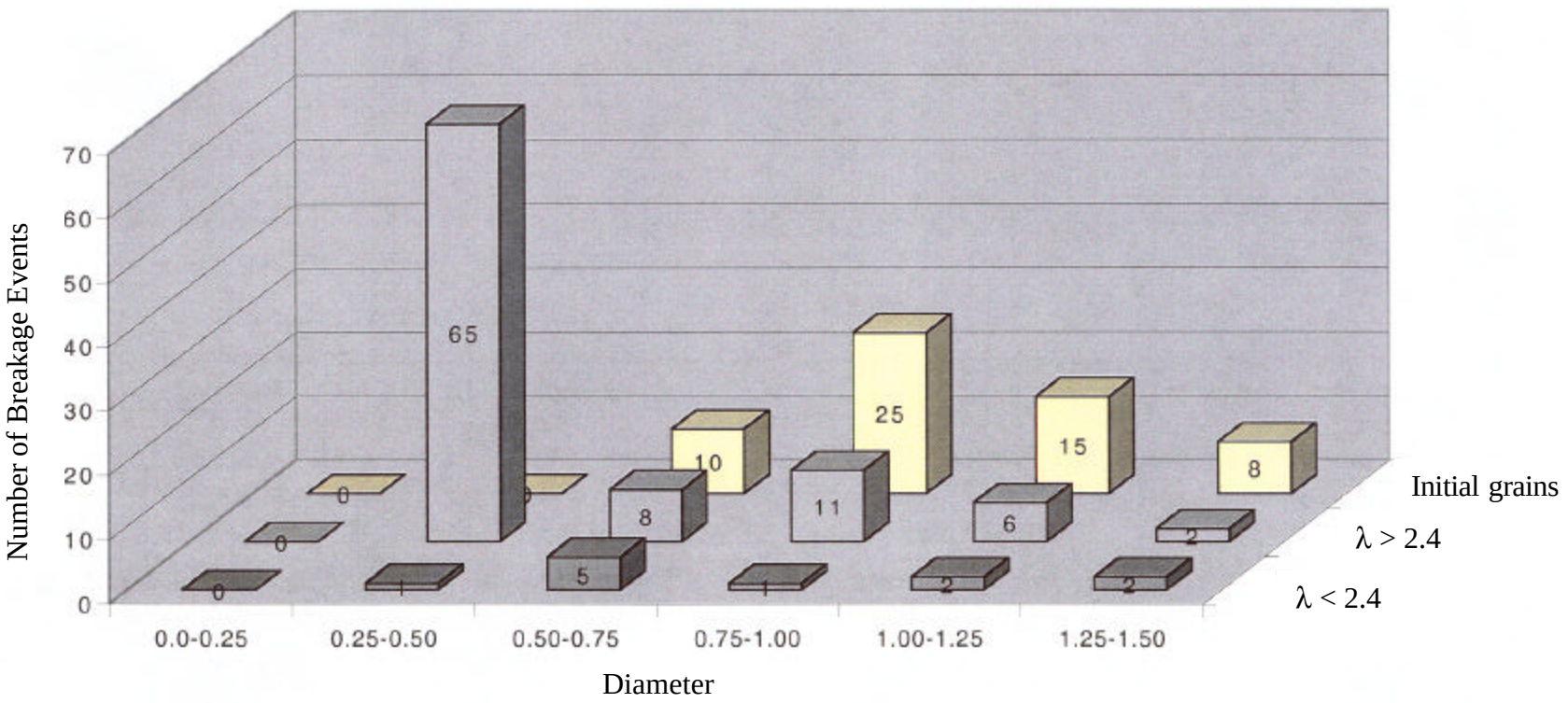


**Figure 16. Histogram of breakage events vs. diameter in R2.0.** Breakage events are binned by the size of the grains that broke and by the displacement (early or late relative to $\lambda$ =2.4). The yellow histogram shows the number of grains in each size bin in the initial system of breakable grains. The numbers on the bars represent the actual number of grains in the bins.

*Porosity evolution*

In models of similar granular systems without grain breakage, the onset of constant velocity shear in a compacted system is accompanied by an increase in porosity. For systems with the Gaussian PSD of the initial one used here, the porosity during shear is about 0.19-0.20, independent of confining stress (Aharanov and Sparks, 2000). So the initial response in each of these systems should be to dilate, with high confining stress runs dilating more. However, grain breakage alters the PSD to allow much more efficient packing, and therefore counters this dilation.

The 2-D porosity data obtained from this research and presented in this sub-section were calculated according to the following formula

$$\text{Porosity} = 1 - \frac{G}{A \cdot B} \qquad (16)$$

with

$$A = \text{Width of the box of grains}$$
$$B = \text{Height of the box of grains}$$
$$G = \text{Total area occupied by grains}$$

Figure 17 shows that once the starting system of grains is subjected to shear, and grain breakage is activated (at Displacement 0 on the horizontal axis), the initial porosity of about 0.16 drops considerably (down to about 0.14) in runs R1.3 and R2.0. In the lower normal stress runs, the porosity increases over the initial value, indicating that not enough breakage and PSD evolution has occurred to offset the shear dilation.

The sporadic occurrence of spikes in the porosity curves of Figure 17 is the effect of large forces occasionally generated when newly-formed grains didn't fit well in the

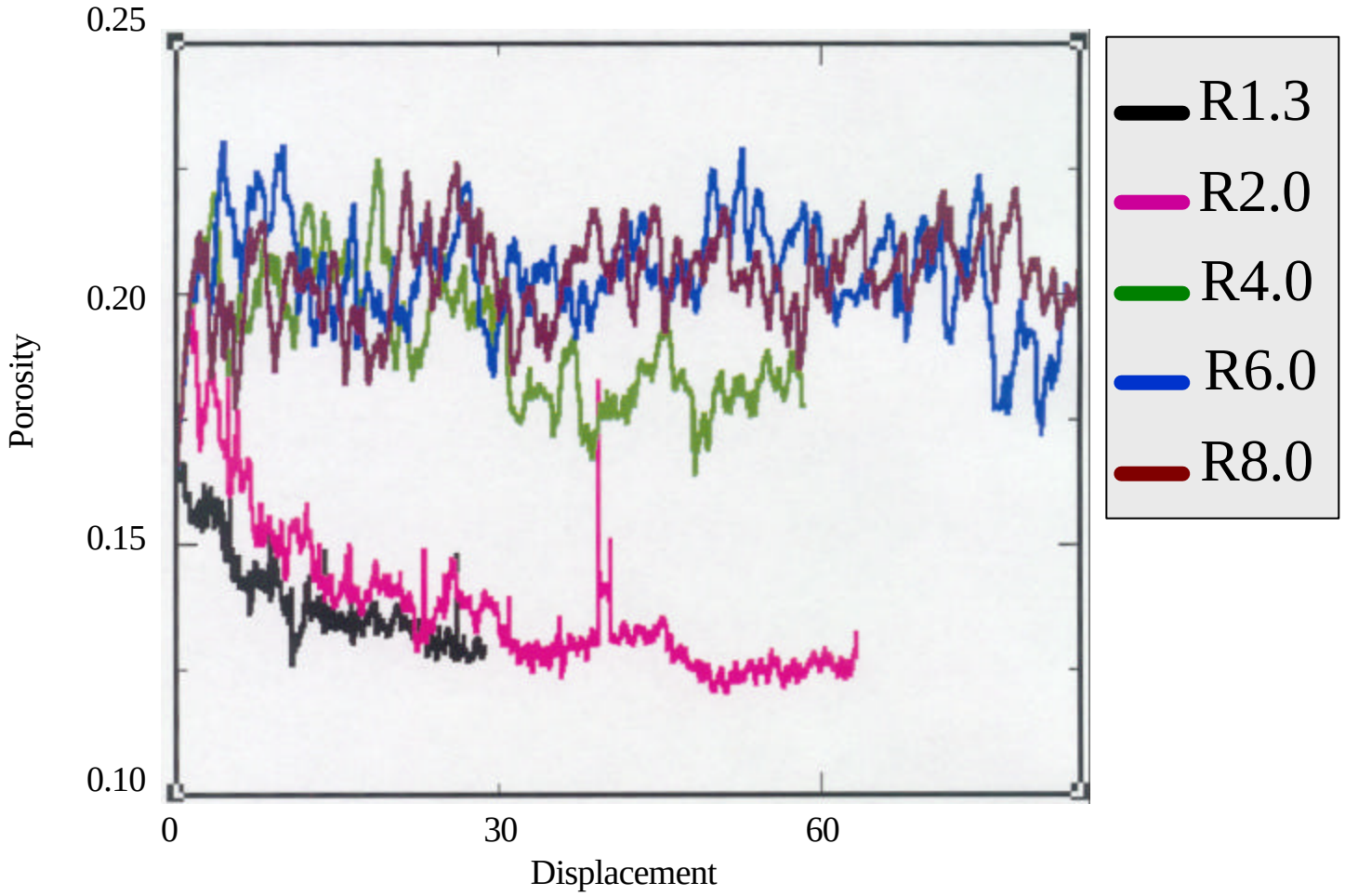


**Figure 17. Porosity evolution.** Porosity evolution with displacement for all the runs.

available pore space (cf. Chapter “Methods” of this thesis). Such forces were rapidly relieved and did not significantly interfere with the trends of the runs.

*Friction*

In the model used, the bulk friction $\mu$ of the layer of gouge is calculated using equation (17) a direct measurement of the total shear force $\bar{\tau}$ on the top wall and the applied normal load N.

$$\mu = \frac{\bar{\tau}}{N} \qquad (17)$$

Figures 18, 19, 20, 21, and 22 show the friction vs. displacement curves for the various runs. There is significant variation with displacement in the measured shear force due to the strong dependence of shear force on continuously changing grain arrangement. Such variations are accentuated in these small systems, which are initially dominated by one or two strong force chains. However, the overall trend of the effective friction is to remain constant or decrease only slightly as the system evolves.

Table 3 shows the parameters of the best-fit linear relationships between friction and displacement, while Table 4 displays the average values of friction for all the numerical simulations.

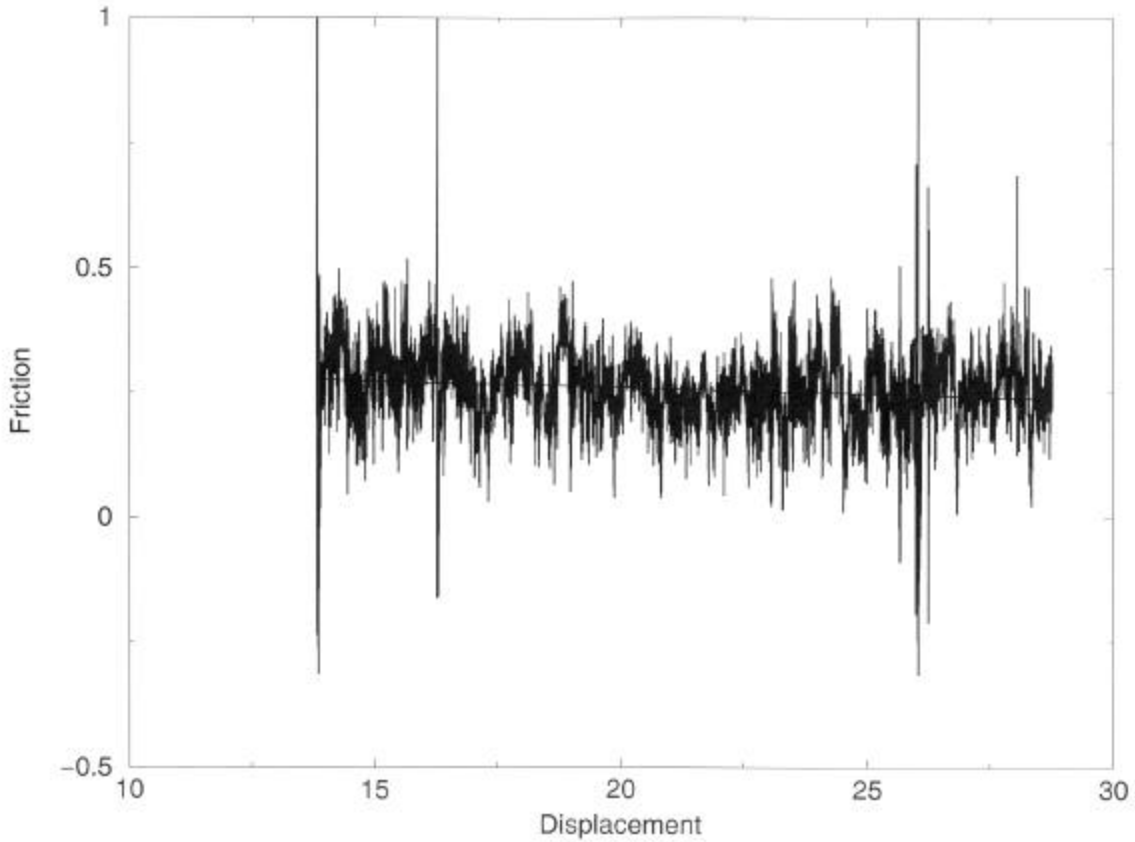


**Figure 18. Friction in R1.3.** Friction versus displacement plot for run R1.3. The data from the beginning to a displacement of about 13 is missing because it got corrupted. The middle straight line represents the best fit of the data.

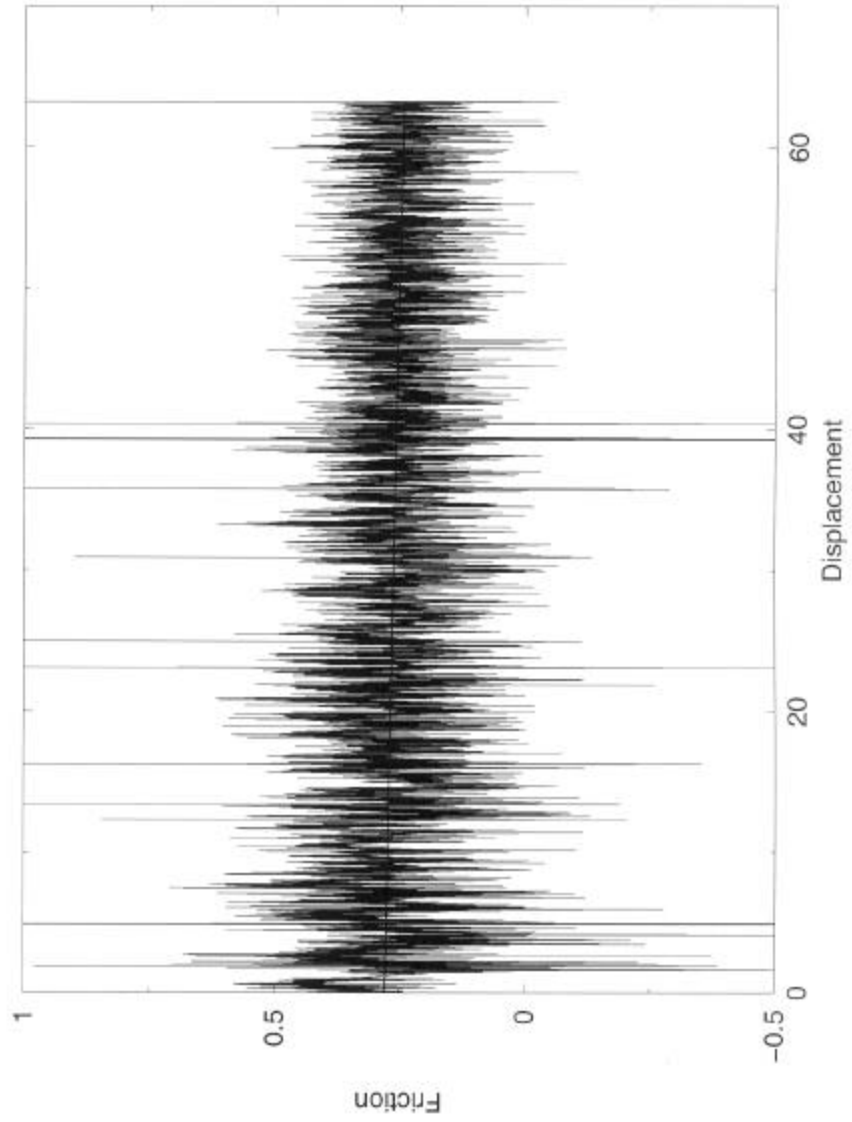


**Figure 19. Friction in R2.0**. Friction versus displacement plot for run R2.0. The middle straight line represents the best fit of the data.

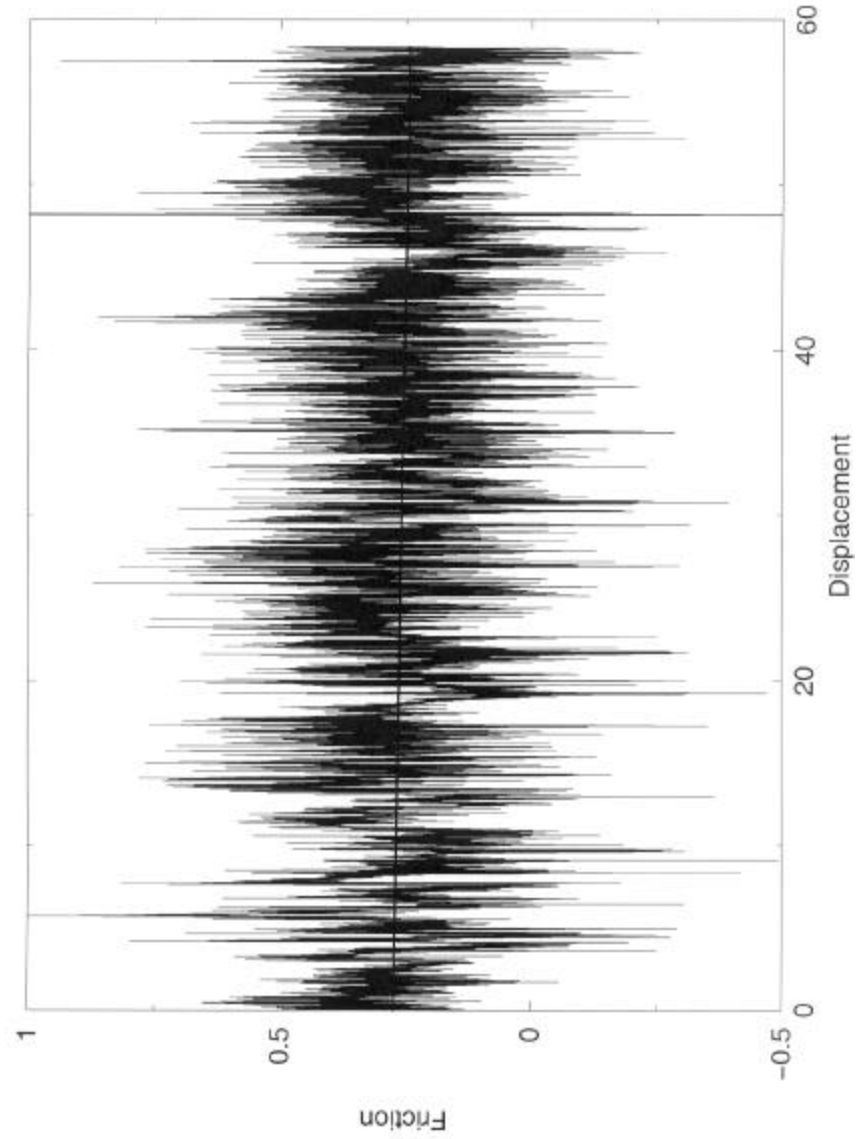


**Figure 20. Friction in R4.0.** Friction versus displacement plot for run R4.0. The middle straight line represents the best fit of the data.

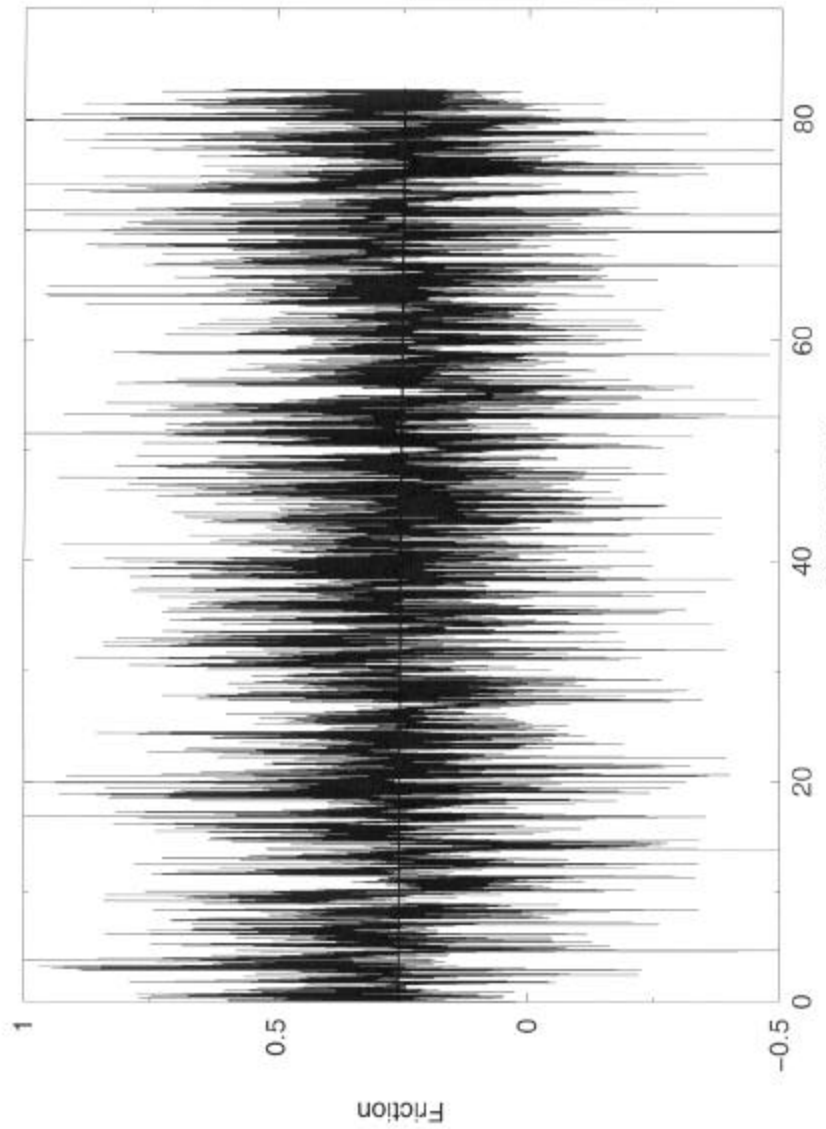


**Figure 21. Friction in R6.0.** Friction versus displacement plot for run R6.0. The middle straight line represents the best fit of the data.

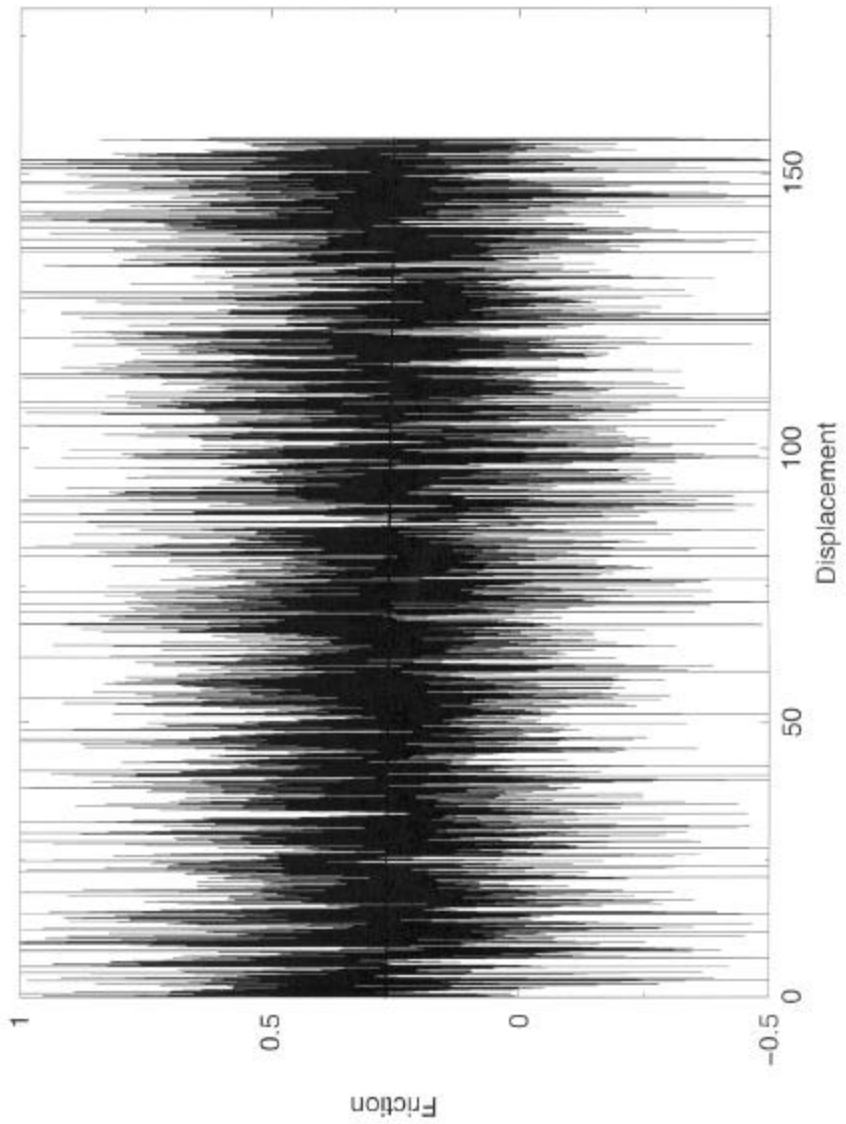


**Figure 22. Friction in R8.0.** Friction versus displacement plot for run R8.0. The middle straight line represents the best fit of the data.

**Table 3.** Regression parameters for friction plots (Figures 18-22)

| RUN | SLOPE | INTERCEPT |
|---|---|---|
| **R1.3** | -2.6E-03 | 0.31 |
| **R2.0** | -5.3E-04 | 0.28 |
| **R4.0** | -5.0E-04 | 0.27 |
| **R6.0** | -1.2E-04 | 0.26 |
| **R8.0** | -1.0E-04 | 0.27 |

**Table 4.** Average friction

| RUN | $\overline{m}$ |
|---|---|
| **R1.3** | 0.2560 |
| **R2.0** | 0.2617 |
| **R4.0** | 0.2538 |
| **R6.0** | 0.2498 |
| **R8.0** | 0.2596 |

In each case, the effective friction appears to be decreasing with continued evolution and it decreases fastest for high-normal stress (greater breakage) runs. The maximum decrease attained however is only of about 0.038. The values of the displacement-averaged friction are identical within the limits of natural variation, with a value of 0.256 ± 0.006.

*Spatial distribution of breakage in run R2.0*

The temporal and spatial variation of the population of the initial grains as well as the populations of the newly formed grains were examined from just one numerical experiment: R2.0, which displayed a moderate amount of grain breakage. The grains

from this run were separated into different populations, labeled by their "generation": the initial 58 grains in the system were defined as Generation 0, the products of breakage of Generation 0 grains comprise Generation 1, and the products of further breakage make up successive generations. Because of the strong limitation imposed by the chosen breakage limit of 0.28, only three generations of grains (Gen 0, Gen 1, and Gen 2) were achieved in this run. At the end of the run, the total number of grains is 670.

At several displacements during the run it was possible to determine the percentage of grains in the system belonging to each generation (Figure 23). Because Gen 0 grains can only be destroyed by breakage, the number of grains of Generation 0 decreases monotonically to 27. Because each broken grain is replaced with seven grains of the next generation, Gen 0 comprises only 4 % of the grains at the end of the run. Note, however, that because of the larger size of Generation 0 grains, this population maintains a significant fraction of the mass in the system. Since the breakage limit does not allow Generation 2 to break, their numbers can only increase during the run. The Generation 1 fraction of the system, whose grains are both produced and destroyed, shows an early increase and then a slow decline.

During the early stage of R2.0 the only grains that could break were in Gen 0. At a displacement of about 2.5, a few breakage events in the Gen 1 population produced a rapid increase in the number of Gen 2 grains. A second episode of Gen 0 breakage produced a second peak in the Gen 1 population around displacement 6.1. From displacement 6.1 on, primarily Gen 1 grains broke, with the rare exception of few Gen 0 grains.

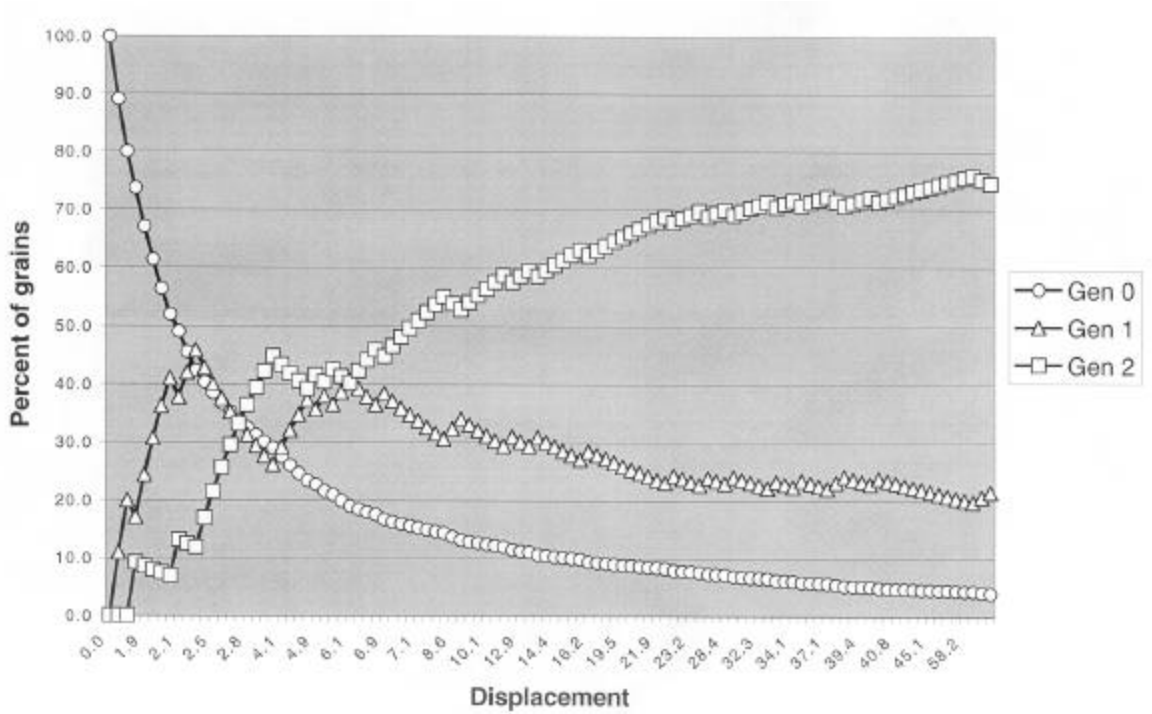


**Figure 23. Generation-displacement plot for R2.0.** At each displacement during run R2.0, the total number of grains in the system was binned into generations and proportions of grains in each generation are plotted here. Note that because of the size difference between the different populations, even a small number of Gen 0 grains still represent a significant fraction of the volume of the system.

The asymptotic trend of Gen 1 indicates that if the simulation were to continue longer, we would likely observe a limited decrease in the rate of breakage of Gen 1 grains.

In order to assess the spatial distribution of breakage, Gen 0, Gen 1, and Gen 2 grains were plotted at different displacements using different colors. Figures 24 and 25 represent the spatial distribution of the populations of grains, respectively, at displacements $\lambda = 6.9$ and $\lambda = 8.6$. By looking at Figure 25, we can identify three "quasi-planar" zones A, B, and C (Figure 26) along which most of the grain crushing have occurred. These three zones are all characterized by high density in Gen 1 and Gen 2 grains indicating multiple cracking and strain localization. A fourth quasi-planar zone of Gen 1 grains, labeled G in the center of Figure 26, illustrates the need to carefully analyze the history of the system before interpreting these features. The origin of this zone is completely different from the ones just discussed in that there was no shear along the plane of the feature. Instead this zone resulted from the upward and downward migration of newly created Gen 1 grains in response to a local force chain that was sub-horizontal.

**Discussion**

The toughest challenge posed by complex granular media is to understand the relationship between the properties of a single grain and the properties of the whole system.

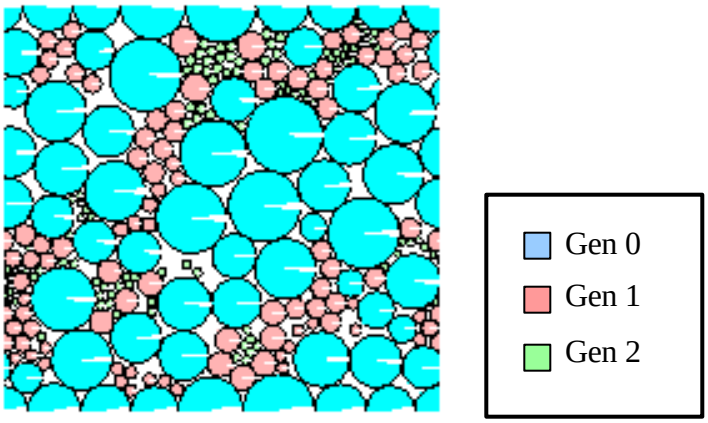


**Figure 24. Spatial distribution of generations of grains in run R2.0 at displacement** $l$ **= 6.9.** Snapshot of the system representing the spatial distribution of Gen 0, Gen 1, and Gen 2 for run R2.0 at displacement 6.9.

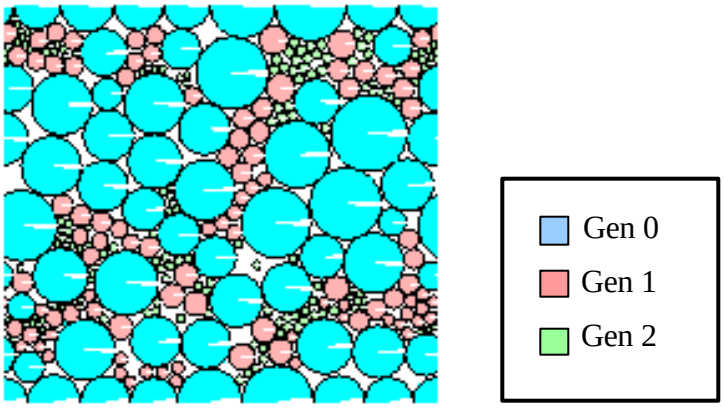


**Figure 25. Spatial distribution of generations of grains in run R2.0 at displacement** $l$ **= 8.6.** Snapshot of the system representing the spatial distribution of Gen 0, Gen 1, and Gen 2 for run R2.0 at displacement 8.6.

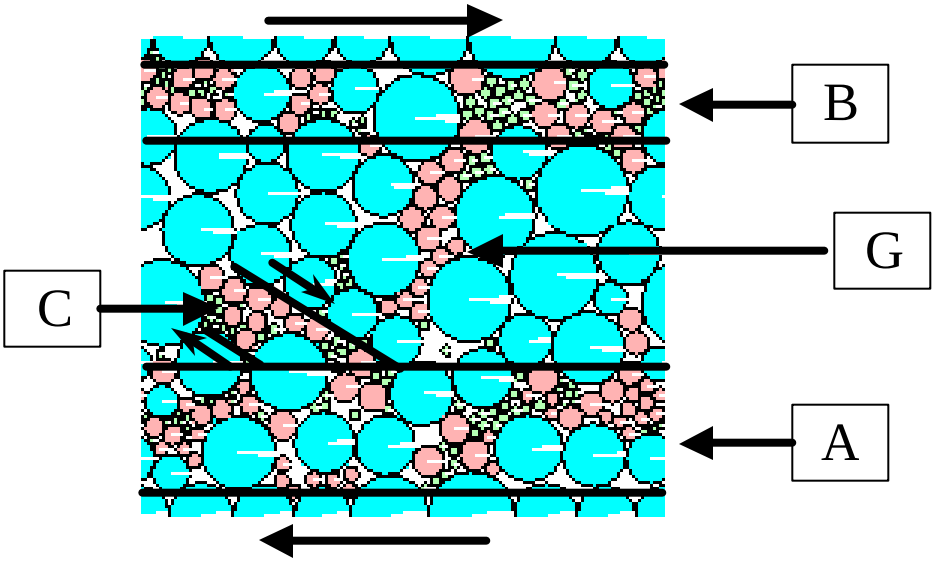


**Figure 26. Localization features in the system of Figure 25.** Interpreted localization features in R2.0 at displacement 8.6. According to my interpretation, A and B are "boundary" shears, and C is a "$R_1$" shear. While the feature labeled G is also a sub-linear region of smaller grains, there has been no motion of the adjacent grains relative to the region.

This section will examine and discuss the results and present some of the insights gained from this research.

The main characteristic displayed by the cumulative breakage-displacement curves shown in Figure 9 is their logarithmic trends, which indicate that grain breakage occurs most rapidly at the beginning of the shearing (especially in R1.3, R2.0, and R4.0) and it slows down with continuous shear deformation. Moreover, the initial rates of breakage differ from one run to the other, being faster for larger confining stresses.

The logarithmic trends of the cumulative breakage-displacement curves are similar to damage associated with wear between two frictional surfaces that slide past each other [see Scholz, 1990 pg. 71]. The initial phase of wear is characterized by fast rates of breakage ("running-in" phase), which decay with increased deformation until the process reaches a quasi-steady-state. An interpretation of this phenomenon is that the running-in phase is related to the removal of the initial excess roughness (i.e. large "asperities") of the surfaces. If greater normal load is applied to the surfaces, there is more contact between the asperities, and the initial wear rate is faster. Once the initial roughness is reduced, the wear rate declines. Similarly, for the simulated gouges of this study, the relatively large initial population of big and inherently weak grains of Gen 0 represents the initial excess roughness. Moreover, the grain breakage rates also are directly related to the confining pressure N. In fact, the larger the confining pressure, the larger the number of highly stressed contacts between big grains. At the beginning of each simulation, the average coordination number (i.e. the average number of grain contacts per grain) is approximately 2.5-3.0. This is controlled primarily by the initial PSD, and

not by the applied confining load. As grains start to break and the PSD evolves and the average coordination number increases until it reaches a plateau around values in the order of 10.0. However, the variance in coordination also grows. The remaining large grains of Gen 0 have quite large coordination numbers ranging on average between 5 and 9; these numerous contact forces promote an internal hydrostatic state of stress, which inhibits breakage and leads to the preservation of these large grains. Conversely, small grains of both Gen 0 and Gen 1 always experience fewer contact forces, which, if large enough, can cause their breakage. Because of the size dependence of grain strength, however, stronger grains are generated and breakage rates decrease steadily leading to the flattening of the cumulative breakage-displacement curves of Figure 9 and to the asymptotic trend of the generation-time curves of Figure 23.

The above inferences agree with the "constrained comminution" model of Sammis et al. [1987] and, to a certain extent, explain and support the interpretation given by Tsoungui et al. [1999] of the "cushioning effect" (i.e. of the internal hydrostatic state of stress) responsible for the survival of large undeformed grains in fault gouges.

In contrast to previous studies, which choose fixed PSDs of "un-breakable" grains [e.g. Aharonov and Sparks, 1999; Morgan, 1999a; Morgan and Boettcher, 1999b], this numerical model allows a system of "breakable" grains to evolve in accordance with established breakage and fragmentation rules. Besides two negligible discrepancies for grain diameters around 0.250 and 0.100 in Figure 12, the PSD for three runs match quite well. This similarity in PDS's also holds for greater degrees of damage (Figures 13, 14, and 15). The fact that Figure 15 shows two virtually identical PSD for runs R1.3 and

R2.0 after 95 grains broke clearly indicates that the PSD follows the same evolutionary path, independent of confining stress and total displacement. Conversely, the main difference between the two runs is represented by the rates of breakage (Figure 9), which indicate that R1.3 reaches the distribution of Figure 15 faster than R2.0. An implication of this result for gouge-filled faults is that after a uniform amount of displacement along a dipping fault, the PSD of the fault gouge would vary with depth (assuming increasing effective normal stress across the fault with depth).

The CBE versus normal load plot (Figure 11) provide insight into how a fault gouge evolves with depth. If one scales the model using an average initial grain size of 1 mm, a Young's modulus of 90 GPa, and a tensile strength of 34 MPa, the calculated confining pressure at which significant breakage initiate is equal to about 7.2 MPa (corresponding to a depth of about 274 m). Therefore, the determination of the above-mentioned critical depth value implies a negligible or absent gouge evolution (with respect to grain breakage) for shallower depths.

Figures 9 and 10 imply that the CBE is directly proportional to the logarithm of a normalized displacement and to a normalized load.

$$CBE = Damage \propto \frac{N - N_0}{T^*} \log\left(\frac{l}{X_0}\right) \qquad (18)$$

Morgan & Boettcher [1999b] pointed out that the shear strength of a fault gouge is highly dependent on the partitioning of the strain between the principal deformation mechanisms. Their simulations could only directly investigate the effects of grain rolling and sliding, while prescribing different PSDs as a proxy for the extent of grain breakage.

According to their analysis, their simulated fault gouges exhibited unstable sliding with a bulk friction ranging between 0.20 and 0.32, and rarely exceeding 0.30. The bulk friction in the models presented in this thesis has an average value of about 0.26. This value agrees well with the results of Morgan & Boettcher [1999b] and Sparks & Aharonov [2000]. These calculated friction values are in disagreement with experimental values of $\mu$ (around 0.60) from shearing of granular materials. In this regard, it must be emphasized that Mair et al's [2000] explanation about the role of grain shape in producing the disagreement might be critical and it calls for further numerical studies using irregular polygonal grains [see Schinner, 1999] in place of circular grains.

Equally interesting is the topic of strain localization in these models. In run R2.0, some zones of smaller grains act as shear localization zones, at least transiently. Such features can be interpreted as typical "boundary" and "$R_1$" Riedel shears (Figure 26), because of their geometry and motion. Since Mair et al [2000] observed that the formation of Riedel shears in their experimentally deformed gouges was directly related to the confining pressure, it can be hypothesized that better defined shear features may develop in the numerically simulated gouges if they are subjected to higher confining stresses than were explored in these runs. Naturally, this hypothesis calls for more "dedicated" runs, which go beyond our goals and time constraints for this project.

# CONCLUSIONS

In the present research project, numerical simulations were employed to study how gouge-filled faults evolve in their internal structures and in their particle size distribution (PSD) as grain breakage and grain rearrangement take place. To achieve the above-stated goal, several new subroutines (in FORTRAN 77), which introduce grain breakage in the code Granfrixl [Aharonov and Sparks, 1999] were designed, implemented, and tested.

In this thesis, the methods and the results obtained from a suite of five 2-D numerical simulations were presented in which the same initial layer of circular grains is subjected to different values of confining pressure and sheared at a constant velocity. In each run, at least a few grains broke during shear, but only in the three highest confining stress runs, do more than 10 grains break. Each of these runs has confining stress above a threshold value, which was estimated to be about 7.2 MPa (assuming quartz grains with average grain size of 1 mm as starting material). The amount of grain breaking increases logarithmically with displacement, with an early running-in phase of more rapid breakage rates followed by a phase of steadily decreasing rates, which may eventually lead to an unbreakable system (not achieved in the duration of the experiments). The initial fast rates of breakage can be related to the breakage of large weak grains. As the grains break, the number of grains in the system and the average coordination number increase. Due to the imposed dependence of tensional strength on grain size, the average strength of grains in the system also increases. These processes are observed to be the

main causes of the reduction in the breakage rates. In fact, while grain breakage proceeds, strong small newly formed grains replace old weaker grains and may endure the transmitted stresses without failing. On the other hand, some large grains survive comminution even though they have relatively low strength, because they are in contact with numerous smaller surrounding grains, which create a more hydrostatic state of stress inside the large grain. Such observations agree well with the “constrained comminution” model of Sammis et al. [1987] and supports the “cushioning effect” described by Tsongui et al. [1999].

Comparing the PSD of different runs after the same number of grains has failed, it was observed that they all have the same distribution regardless the applied confining pressures or resulting breakage rates. The similarity between the cataclastic evolutions of all the runs implies that we should expect different degrees of comminution and structure along a vertical fault with uniform displacement. In the simulations performed in this study, some shearing planes in run R2.0 were also recognized, which might be interpreted as Riedel shears. However, probably higher confining pressures than those here explored are necessary to clearly observe the formation and preservation of localized shear features.

# REFERENCES

Aharonov, E., and D. Sparks, Rigidity phase transition in granular packings, *Phys. Rev. E, 60*, No. 6, 6890-6896, 1999.

An, L., and C.G. Sammis, Particle size distribution of cataclastic fault materials from Southern California: a 3-D study, *Pure and Appl. Geophys., 143*, 203-227, 1994.

Åström, J.A., and H.J. Herrmann, Fragmentation of grains in a two-dimensional packing, *Eur. Phys. J. B, 5*, 551-554, 1998.

Åström, J.A., H.J. Herrmann, and J. Timonen, Granular packings and fault zones, *Phys. Rev. Lett., 84*, No. 4, 638-641, 2000.

Berg, R.R., and A.H. Avery, Sealing properties of Tertiary growth faults, Texas Gulf Coast, *AAPG Bull., 79*, No. 3, 375-393, 1995.

Biegel, R.L., C.G. Sammis, and J.H. Dieterich, The frictional properties of a simulated gouge having a fractal particle distribution, *J. Struct. Geol., 11*, 827-846, 1989.

Blenkinsop, T.G., Cataclasis and processes of particle size reduction, *Pure and Appl. Geophys., 136*, 59-86, 1991.

Blenkinsop, T.G., and T.R.C. Fernandes, Fractal characterization of particle size distributions in chromitites from the Great Dyke, Zimbabwe, *Pure and Appl. Geophys., 157*, 505-521, 2000.

Buchholtz, V., J.A. Freund, and T. Pöschel, Molecular dynamics of comminution in ball mills, *Euro. Phys. Journ. B, 16*, 169-182, 2000.

Cates, M.E., J.P. Wittmer, J.P. Bouchaud, and P. Claudin, Jamming and stress propagation in particulate matter, *Physica A, 263*, 354-361, 1999.

Cladouhos, T.T, Shape preferred orientations of survivor grains in fault gouge, *J. Struct. Geol.*, *21*, 419-436, 1999.

Cundall, P.A., and O.D.L. Strack, A discrete numerical model for granular assemblies, *Géotechnique*, *29*, No. 1, 47-65, 1979.

Donzé, F., P. Mora, and S.A. Magnier, Numerical simulation of faults and shear zones, *Geophys. J. Int.*, *116*, 46-52, 1994.

Engelder, J.T., Cataclasis and the generation of fault gouge, *Geol. Soc. Am. Bull.*, *85*, 1515-1522, 1974.

Fisher-Cripps, A.C., *Introduction to Contact Mechanics*, Springer, New York, 2000.

Gallagher, J.J., Fracturing of quartz sand grains, *Proceedings of 17th Symposium on Rock Mechanics, Snowbird, Utah, August 25-27*, 1976.

Gallagher, J.J., M. Friedman, J. Handin, and G.M. Sowers, Experimental studies relating to microfracture in sandstone, *Tectonophysics*, *21*, 203-247, 1974.

Granick, S., Soft matter in a tight spot, *Physics Today*, *52*, No. 7, 26-31, 1999.

Hattori, I., and H. Yamamoto, Rock fragmentation and particle size in crushed zones by faulting, *J. Geology*, *107*, 209-222, 1999.

Hoffmann, N., and K. Schönert, Bruchanteil von glaskugeln in packungen von franktionen and binären mischungen, *Aubereit. Tech.*, *12*, 513-518, 1971.

Kendall, K., The impossibility of comminuting small particles, *Nature*, *272*, 710-711, 1978.

Mair, K., K. Frye, and C. Marone, Effect of gouge characteristics on the strength and stability of faults (abstract), *Eos Trans. AGU, 81*, F1132, 2000.

Mandl, G., L.N.J. de Jong, and A. Maltha, Shear zones in granular material. An experimental study of their structure and mechanical genesis, *Rock Mechanics*, *9*, 95-144, 1977.

Marone, C., and C.H. Scholz, Particle-size distribution and microstructures within simulated fault gouge, *J. Struct. Geol.*, *11*, No. 7, 799-814, 1989.

Michibayashi, K., The role of intragranular fracturing on grain size reduction in feldspar during mylonitization, *J. Struct. Geol.*, *18*, No. 1, 17-25, 1996.

Morgan, J.K., Numerical simulations of granular shear zones using the distinct element method. 2. Effects of particle size distribution and interparticle friction on mechanical behavior, *J. Geophys. Res.*, *104*, No. B2, 2721-2732, 1999a.

Morgan, J.K., and M.S. Boettcher, Numerical simulations of granular shear zones using the distinct element method. 1. Shear zone kinematics and micromechanics of localization, *J. Geophys. Res.*, *104*, No. B2, 2703-2719, 1999b.

Mueth, D.M., H.M. Jaeger, and S.R. Nagel, Force distribution in a granular medium, *Phys. Rev. E*, *57*, 3164-3169, 1998.

Muskhelishvili, N.I., *Some Basic Problems of the Mathematical Theory of Elasticity*, P.Noordhoff Ltd, Groningen, The Netherlands, 1963.

Pittman, E.D., Effect of fault-related granulation on porosity and permeability of quartz sandstones, Simpson Group (Ordovician), Oklahoma, *AAPG Bull.*, *65*, No. 11, 2381-2387, 1981.

Place, D., and P. Mora, Numerical simulation of localization phenomena in a fault zone, *Pure and Appl. Geophys.*, *157*, 1821-1845, 2000.

Prasher, C.L., *Crushing and Grinding Process Handbook*, John Wiley & Sons, New York, 1987.

Rapaport, D.C., *The Art of Molecular Dynamics Simulation*, Cambridge University Press, New York, 1997.

Sammis, C.G., and R.L. Biegel, Fractals, fault-gouge, and friction, *Pure and Appl. Geophys.*, *131*, 255-271, 1989.

Sammis, C.G., and S.J. Steacy, The micromechanics of friction in a granular layer, *Pure and Appl. Geophys.*, *142*, 777-794, 1994.

Sammis, C.G., G. King, and R. Biegel, The kinematics of gouge deformation, *Pure and Appl. Geophys.*, *125*, 777-812, 1987.

Sammis, C.G., R.H. Osborne, J.L. Anderson, M. Banerdt, and P. White, Self-similar cataclasis in the formation of fault gouge, *Pure and Appl. Geophys.*, *124*, 53-78, 1986.

Schinner, A., Fast algorithms for the simulation of polygonal particles, *Granular Matter*, *2*, No. 1, 35-43, 1999.

Scholz, C.H., *The Mechanics of Earthquakes and Faulting*, Cambridge University Press, New York, 1990.

Steier, K., and K. Schönert, Verformung und bruchphänomene unter druckbeanspruchung von sehr kleinen körnern aus kalkstein, quartz und polystyrol, *Dechema Monograph*, *69*, 167-192, 1972.

Tsongui, O., D. Vallet, and J.C. Charmet, Numerical model of crushing of grains inside two-dimensional granular materials, *Powder Tech.*, *105*, 190-198, 1999.

# APPENDIX

Section from main routine.

```
*****************************************************************
*                     BREAKING GRAINS                           *
*****************************************************************


C The following subroutines are called when a particle  breaks
C and the pieces are re-arranged. Notice that the do-loop uses
C fake time steps

          call principalstress

           do i=1,ngrains
            k=nglist(i)
            teindx(k)=0.
            stot(k)=0.
           enddo
        do ik=1,kcont
            i=cont_i(ik)
            j=cont_j(ik)
            olap(ik)=sqrt(cont_fn(ik)*cont_fn(ik)+
     1            cont_ft(ik)*cont_ft(ik))
              stot(i)=stot(i)+cont_fn(ik)
              stot(j)=stot(j)+cont_fn(ik)
           enddo

           maxstr=0.
           part=0
           tx=0.
           do i=1,ngrains
            k= nglist(i)
             if (bdgrain(k) .EQ. 0) then
              ff=sqrt(fx(k)*fx(k)+fy(k)*fy(k))
              if (radius(k) .gt. 0.14 .AND.
     1            ff.LT.(0.5*abs(stot(k)))) then
               tx=sigmax(k)-strgth(k)
               teindx(k)=tx
               if (tx .GT. maxstr) then
                maxstr=tx
                part=k
               endif
              else
               teindx(k)=100.
              endif
             endif
           enddo

          if (crush.EQ.1) then
```

```
          stepf=0


              if (part .GT. 0) then
               ibreak=part
               tempof=tau+100.
               goto 321
              else
               goto 326
              endif

321    nevent=nevent+1
            print*, 'Plotting before grain break at STEP ',step
              next=next+1
            print*, 'FRAME =',next
              call pscriptplot(next,presx,presy,igif,fnn)
              call writeint(fnn)

      masskept=0.92
      grainarea=grainarea-(1.-masskept)*pi*radius(ibreak)**2
       call breaks (RX,RY,RADIUS,vx,vy,pieces,ibreak,nglist,MAXN,
     1 newgrn,rnew,radinv2,color,masskept)

       write(60,501) tau,ibreak,2.0*radius(ibreak)
501    format(1x,e15.4,1x,I5,1x,e15.4)

          call breaksetup(ibreak,mx,my,rx(ibreak),ry(ibreak),
     1         xright,xleft,ybot,ytop,kcell,bmap)
*

            do i=ngrains-5,ngrains
             teindx(i)=teindx(ibreak)
            enddo
C Change time step dt
            if (rnew .LT. rsmall) then
c             pause 'im trying to reset the time step'
             dt=dt*((rnew/rsmall)**1.5)
             rsmall=rnew
            endif
*
*
            print*, 'time step=',dt

              conto1=0
              conto2=0
             call movean(fytop,fybot,pieces,newgrn)
             call breakforce(fbx,fby,ibreak,kcell,newgrn,pieces,bmap)
             call movebn(FYTOP, FYBOT,pieces,newgrn)

           tol=1.0e-7
           do 206 itf=1,1000
```

```
            call movean(fytop,fybot,pieces,newgrn)
            call breakforce(fbx,fby,ibreak,kcell,newgrn,pieces,bmap)
            call movebn(FYTOP,FYBOT,pieces,newgrn)
 206       continue

           do 209 itf=1,300000

            call movean(fytop,fybot,pieces,newgrn)
            call breakforce(fbx,fby,ibreak,kcell,newgrn,pieces,bmap)
            call movebn(FYTOP,FYBOT,pieces,newgrn)

            do j=1,pieces
             k=newgrn(j)
             f2(j)=fx(k)*fx(k)+fy(k)*fy(k)
             if (f2(j) .gt. .01*tol*tol) goto 209
            enddo
            goto 210

 208        do j=1,pieces
             k=newgrn(j)
             v2(j)=vx(k)*vx(k)+vy(k)*vy(k)
             if (v2(j) .gt. tol*tol) goto 209
            enddo
            goto 210

 209        continue

 210        continue

          print*, 1000+itf,' fake time steps'
            print*, (sqrt(f2(j)),j=1,7)

 505       format(1x,I5,8(1x,e15.4))
 506       format(8(1x,e15.4))

            do j=1,pieces
             k=newgrn(j)
             vx(k)=0.
             vy(k)=0.
            enddo

            call links
            call force(gx, gy, ev, presx, presy, fytop, fybot,
     1        fxtop,fxbot,fbx,fby,ipfc)
            call principalstress
            crush=0

            print*, 'Plotting after grain break at STEP ',step
              next=next+1
            print*, 'FRAME =',next
              call pscriptplot(next,presx,presy,igif,fnn)
              call writeint(fnn)
```

```
          endif


         if (crush1 .EQ. 1) then
          if (tau .GE. tempof) then
           crush=1
          endif
         endif

*****************************************************************
*                    END OF BREAKING GRAINS                     *
*****************************************************************




*STRENGTH*********************************************
*This subroutine assignes strength to the grain i    *
*according to a switch. So, if                       *
*typest=0                                            *
*all the grains have the same strength regardless    *
*regardless thier size                               *
*                                                    *
*typest=1                                            *
*the grains have a size-dependent strength and a     *
*random component                                    *
*                                                    *
*typest=2                                            *
*the grains have only a size-dependent strength      *
*                                                    *
*typest=3                                            *
*the grains have only a random strength              *
*                                                    *
*Variables used:                                     *
*i : grain index                                     *
*randnm : random number between 0 and 1              *
*A,B : coefficients                                  *
*typest : switch for type of strength                *
*purest : min. possibile strength                    *
*esp : esponent used for the strength-size dependence*
*strgth : strength of the grains                     *
*                                                    *
*Input : i,randnm,typest,esp,purest,radius           *
*Output : strgth                                     *
*Programmer: Richard A. Lang                         *
*****************************************************
        SUBROUTINE STRENGTH(i,randnm)

        include 'mycommons'

        integer  i
        real*8   A,B,randnm
```

```
*-----------------------------------------------------*
        if (typest .EQ. 0) then
         A=0.
         B=0.
        elseif (typest .EQ. 1) then
         A=1.
         B=1.
        elseif (typest .EQ. 2) then
         A=1.
         B=0.
        else
         A=0.
         B=1.
        endif

        strgth(i)=purest+(A*purest)/((2.0*radius(i))**esp)+
     & (B*purest*100.0*randnm)

        end




*BREAKS*************************************************************
***
*
*
*This program breaks a chosen particle in a prefixed number of pieces
*
*
*
*Variables used:
*
*pieces : Number of pieces in which a particle breaks
*
*m,i : Indices
*
*rnew : Radius of the broken particles
*
*x,y,r : Coordinates, and radius the particles
*
*nglist : Index of atom
*
*MAXN : Maximum number of particles
*
*x1,y1,r1,x2,y2,r2,x3,y3,r3
*
*x4,y4,r4,x5,y5,r5,x6,y6,r6 : Dummy variables
*
```

```
*newgrn : Array of index of newly-formed particles
*      *
*
*Input : x,y,r (before breaking),pieces,n,m,nglist,MAXN
*
*
*
*Output : x,y,r (after breaking),rnew,MAXN,nglist
*
*
*
*
*
*Programmer : Richard A. Lang
*
*
*
**********************************************************************
***
      SUBROUTINE BREAKS(x,y,r,u,v,pieces,m,nglist,MAXN,
     1  newgrn,rnew,radinv2,color,masskept)
      integer MAXN,nglist(MAXN),newgrn(7),pieces,t,i,m
      real*8 rnew,x(MAXN),y(MAXN),r(MAXN),radinv2(MAXN)
      real*8 u(MAXN),v(MAXN)
      integer color(MAXN)
      real*8 x1,y1,r1,x2,y2,r2,x3,y3,r3,x4,y4,r4
      real*8 x5,y5,r5,x6,y6,r6
      integer k
      real*8 masskept



       do i=1,7
        newgrn(i)=0
       enddo
*
*
* Break the particle in pieces, calculate new radii, and create
* an array with the newly-formed particles
       print*
       m=nglist(m)
       print*,'PARTICLE ',m,' BREAKS INTO',pieces,' PIECES!'
c  masskept=fraction of original particle mass that goes into the
c     new pieces (rest is lost)
       rnew=r(m)*sqrt(masskept/real(pieces))

       print*, 'NEW RADIUS = ',rnew
       if (pieces.EQ.3) then
        x1= x(m)
        y1= y(m)+(rnew/0.86602540)
        r1= rnew
        call addgrain3(x1,y1,r1,1,0,t)
        newgrn(1)=t
        color(newgrn(1))=6
```

```
  x2= x(m)+rnew
  y2= y(m)-(0.57735027*rnew)
  r2= rnew
  call addgrain3(x2,y2,r2,1,0,t)
  newgrn(2)=t
  color(newgrn(2))=6
  x(m)= x(m)-rnew
  y(m)= y(m)-(0.57735027*rnew)
  r(m)= rnew
      radinv2(m)=.25/(r(m)*r(m))
  newgrn(3)=m
  color(newgrn(3))=6
 end if

if (pieces .EQ. 7) then
  x1= x(m)-(2.0*rnew)
  y1= y(m)
  r1= rnew
  call addgrain3(x1,y1,r1,1,0,t)
  newgrn(1)=t
  color(newgrn(1))=6
  x2= x(m)-rnew
  y2= y(m)+(1.73205081*rnew)
  r2= rnew
  call addgrain3(x2,y2,r2,1,0,t)
  newgrn(2)=t
  color(newgrn(2))=6
  x3= x(m)+rnew
  y3= y(m)+(1.73205081*rnew)
  r3= rnew
  call addgrain3(x3,y3,r3,1,0,t)
  newgrn(3)=t
  color(newgrn(3))=6
  x4= x(m)+(2.0*rnew)
  y4= y(m)
  r4= rnew
  call addgrain3(x4,y4,r4,1,0,t)
  newgrn(4)=t
  color(newgrn(4))=6
  x5= x(m)+rnew
  y5= y(m)-(1.73205081*rnew)
  r5= rnew
  call addgrain3(x5,y5,r5,1,0,t)
  newgrn(5)=t
  color(newgrn(5))=6
  x6= x(m)-rnew
  y6= y(m)-(1.73205081*rnew)
  r6= rnew
  call addgrain3(x6,y6,r6,1,0,t)
  newgrn(6)=t
  color(newgrn(6))=6
  r(m)=rnew
  radinv2(m)=.25/(r(m)*r(m))
  newgrn(7)=m
```

```
        color(newgrn(7))=6
       end if
*
        print*
        print*, 'I BROKE PARTICLE ',m,' in ',pieces,' PIECES'
*
        do k=1,7
         u(newgrn(k))=0.
         v(newgrn(k))=0.
        enddo

      end
*-------------------------------------------------------*




*STRESS*************************************
*This subroutine calculates the quantities u1,*
*u2,u3 whenever two particles m,i interact    *
*Such quantites are used to calculate the     *
*stress tensor at the center of the particles *
*in the subroutine Principalstress            *
*                                             *
*Variables used:                              *
*m,i : particles indices                      *
*xm,ym,xi,yi : x and y components of forces   *
*radius : radius of particles                 *
*eta,beta,omega,zeta,mu : angles between      *
*interparticle forces and x-axis              *
*dm,em,fm,gm : sin and cos for particle m     *
*di,ei,fi,gi : sin and cos for particle i
*u1,u2,u3 : arrays used for the calculation   *
*of stress tensor                             *
*                                             *
*Input : m,i,xm,ym,xi,yi,radius,u1,u2,u3      *
*                                             *
*Output : Updated u1,u2,u3                    *
*                                             *
*Programmer : Richard A. Lang                 *
*********************************************
      SUBROUTINE STRESS(m,i,xm,ym,xi,yi)

      include 'mycommons'

      integer m,i
      real*8 xm,ym,xi,yi,eta,beta,omega,zeta,mu
      real*8 PI,dm,em,fm,gm,di,ei,fi,gi


*-------------------------------------------------------*
      PI=3.1415927
```

```
eta=0.
beta=0.
mu=0.
omega=0.
zeta=0.
dm=0.
em=0.
fm=0.
gm=0.
di=0.
ei=0.
fi=0.
gi=0.

  if (rx(m) .EQ. rx(i)) then
   if (ry(m) .LT. ry(i)) then
    eta=0.5*PI
    beta=1.5*PI
   else
    eta=1.5*PI
    beta=0.5*PI
   endif
  elseif (ry(m) .EQ. ry(i)) then
   if (rx(m) .LT. rx(i)) then
    eta=0.
    beta=PI
   else
    eta=PI
    beta=0.
   endif

  else
  omega=atan(abs((ry(m)-ry(i))/(rx(m)-rx(i))))
   if (rx(m) .LT. rx(i)) then
    if (ry(m) .LT. ry(i)) then
     eta=omega
     beta=PI+omega
    else
     eta=2.0*PI-omega
     beta=PI-omega
    endif
   else
    if (ry(m) .LT. ry(i)) then
     eta=PI-omega
     beta=2.0*PI-omega
    else
     eta=PI+omega
     beta=omega
    endif
   endif
  endif

zeta= 3.0*eta
mu=3.0*beta
```

```
      dm=sin(eta)
      em=cos(eta)
      fm=sin(zeta)
      gm=cos(zeta)
      di=sin(beta)
      ei=cos(beta)
      fi=sin(mu)
      gi=cos(mu)

      u1(m)=u1(m)+(xm*em+ym*dm)/(PI*radius(m))
      u2(m)=u2(m)-(xm*(em+gm)+ym*(fm-dm))/
     1   (PI*radius(m))
      u3(m)=u3(m)+(xm*(dm+fm)+ym*(em-gm))/
     1   (PI*radius(m))

      u1(i)=u1(i)+(xi*ei+yi*di)/(PI*radius(i))
      u2(i)=u2(i)-(xi*(ei+gi)+yi*(fi-di))/
     1   (PI*radius(i))
      u3(i)=u3(i)+(xi*(di+fi)+yi*(ei-gi))/
     1   (PI*radius(i))


      end
*-----------------------------------------------------------------------
-*




*PRINCIPALSTRESS*****************************************
*This subroutine calculates the principal stresses at the *
*center of the grains                                     *
*                                                        *
*Variables used :                                        *
*u1,u2,u3 : arrays calculated in subroutine "stress"      *
*b,c : coefficients of the quadratic equation             *
*sigxx,sigyy,sigxy : coefficients of the stress matrix at *
*the center of the grains                                 *
*l1,l2 : eigenvalues of the stress tensor                 *
*cron : angle from x-axis to max principal stress sigmax  *
*sigmax,sigmin : max and min principal stresses at the    *
*center of the grains                                     *
*                                                        *
*Input : u1,u2,u3                                        *
*                                                        *
*Output : sigmax,sigmin,l1,l2,cron                       *
*                                                        *
*Programmer : Richard A. Lang                            *
*********************************************************
      SUBROUTINE PRINCIPALSTRESS

      include 'mycommons'
```

```
      integer k,i
      real*8 q,f
      real*8 sigxx(MAXN),sigyy(MAXN),sigxy(MAXN)
      real*8 b(MAXN),c(MAXN)
      real*8 pi

      pi=4.*atan(1.)

*-------------------------------------------------------------*
      f=0.
      q=0.
      do i=1,NGRAINS
       k=nglist(i)
       sigxx(k)=0.
       sigyy(k)=0.
       sigxy(k)=0.
       sigmax(k)=0.
       sigmin(k)=0.
       cron(k)=0.
       l1(k)=0.
       l2(k)=0.
       b(k)=0.
       c(k)=0.
      enddo


       do i=1,NGRAINS
        k=nglist(i)
        sigxx(k)= 0.5*(u1(k)-u2(k))
        sigyy(k)= 0.5*(u1(k)+u2(k))
        sigxy(k)= 0.5*u3(k)
       enddo

        do i=1,NGRAINS
         k=nglist(i)
        if (coordn(k) .GE. 2) then
         b(k)= -(sigxx(k)+sigyy(k))
         c(k)= -((sigxy(k)*sigxy(k))-(sigxx(k)*sigyy(k)))
         f= sqrt((b(k)*b(k))-(4.0*c(k)))
         f=sign(f,b(k))
         q=-0.5*(b(k)+f)
         l1(k)=q
         l2(k)=c(k)/q

         if (l1(k) .GE. l2(k)) then
           sigmax(k)=l1(k)
           sigmin(k)=l2(k)
          else
           sigmax(k)=l2(k)
           sigmin(k)=l1(k)
          endif

         if (sigxy(k) .EQ. 0.) then
```

```
           cron(k)=0.5*PI
          else
           cron(k)=atan((sigmax(k)-sigxx(k))/sigxy(k))
          endif

        else
         sigmax(k)= 0.
         sigmin(k)=0.
         cron(k)=0.
        endif


        enddo

      end
*-----------------------------------------------------------------*
```

# VITA

Richard Anthony Lang

2900 Pearland Pky #11201 Phone: (281) 412-0192

Pearland, TX 77581 ral8863@geo.tamu.edu

## Education

Texas A & M University, College Station, TX.

Master of Science in Geophysics. GPA 3.850, 5/02.

University “La Sapienza” Rome-Italy.

Bachelor of Science in Geology (“Summa cum Laude”), 5/96.

## Publications

Caputo M., Lang R.A., & Esposito L., The stress field of the crust in the Piombino-Cesenatico Northern Apennine section, Mem. Soc. Geol. It., 52, 247-257, 1998.

Lang R.A. & Tucci P., A preliminary study of the causes of the blackening of pebbles in the Cenomanian “Breccia with Black Pebbles” of Camporosello (Lepini Mountains-Italy), Geologica Romana, 33, 89-97, 1997.

## Abstracts

Lang, R. & Sparks D.W., submitted to EOS Trans. Amer. Geophys., March, 2001.